October 2017

Effects of Malformed or Absent Valves to Lymphatic Fluid Transport and Lymphedema in Vivo in Mice

Akshay S. Pujari
University of Massachusetts Amherst

EFFECTS OF MALFORMED OR ABSENT VALVES TO LYMPHATIC FLUID TRANSPORT AND LYMPHEDEMA *IN VIVO* IN MICE

A Thesis Presented

by

AKSHAY S. PUJARI

Submitted to the Graduate School of the
University of Massachusetts Amherst in partial fulfillment
of the requirements for the degree of

MASTER OF SCIENCE

September 2017

Department of Mechanical and Industrial Engineering

EFFECTS OF MALFORMED OR ABSENT VALVES TO LYMPHATIC FLUID TRANSPORT AND LYMPHEDEMA *IN VIVO* IN MICE

A Thesis Presented

by

AKSHAY S. PUJARI

Approved as to style and content by:

_____
Juan Jiménez, Chair

_____
Yubing Sun, Member

_____
Maureen Lynch, Member

_____
Dr. Sundar Krishnamurty,
Department Head
Department of Mechanical and Industrial Engineering

DEDICATION

To Aai, Baba and Rucha.

ACKNOWLEDGMENTS

I would like to thank my advisor Professor Juan M. Jiménez for his advice, support and patience during the creation of this thesis. I could not have asked for a better advisor, and I truly appreciate all that he has done for me. Transitioning from the field of mechanical engineering to study of vascular biology, performing experiments with tissues was a challenging, yet interesting task and I thank him for constantly motivating me to learn new things – both simple and challenging. I would additionally like to thank my advisor for creating a stimulating lab environment and for weekly journal club and manuscript review lab meetings.

I would like to thank all my lab mates for their support, help and feedback to my work and their willingness to read and listen. Special mention to Kin Chau who helped this study by doing tedious work of manual particle tracking and for finding time in his busy schedule. I would like to extend my thanks to Alex Smith for generating particle tracking data. I would also like to thank our lab manager Mary Hagen for all her help conducting immunohistochemistry experiments and her guidance. I would also like to acknowledge the use of the microscopy facility and Imaris software access within the Peyton research group in Department of Chemical Engineering, University of Massachusetts Amherst.

Finally, thank you to my family and friends for all their encouragement, support. I would like to thank my parents Sanjeev and Seema and my sister Rucha for being my constant pillars and supporting me throughout, even while currently being 8000 miles away from me.

ABSTRACT

EFFECTS OF MALFORMED OR ABSENT VALVES TO LYMPHATIC FLUID TRANSPORT AND LYMPHEDEMA *IN VIVO* IN MICE

SEPTEMBER 2017

AKSHAY S. PUJARI

BACHELOR OF ENGINEERING, SHIVAJI UNIVERSITY, INDIA

MASTER OF SCIENCE, UNIVERSITY OF MASSACHUSETTS AMHERST

Directed by: Professor Juan M. Jiménez

Lymph is primarily composed of fluid and proteins from the blood circulatory system that drain into the space surrounding cells, interstitial space. From the interstitial space, the fluid enters and circulates in the lymphatic system until it is delivered into the venous system. In contrast to the blood circulatory system, the lymphatic system lacks a central pumping organ dictating the predominant driving pressure and velocity of lymph. Transport of lymph via capillaries, pre-collecting and collecting lymphatic vessels relies on the synergy between pressure gradients, local tissue motion, valves and lymphatic vessel contractility. The direction of lymph transport is regulated by bicuspid valves distributed throughout pre-collecting and collecting lymphatic vessels.

Effective transport of lymph into the venous system is of prime importance. Disruption of lymph transport, because of impaired lymphatic function, reduced numbers of vessels or valvular insufficiencies can have severe health consequences, including lymphedema for which current clinical therapies are not curative. The lymphatic valves are usually bicuspid, however, congenital malformations in the valve such as single

leaflet valve formation and arrested lymphatic valve development are observed and can cause lymphedema.

Here we employ 4-week-old mice to study the effects of valves and malformed valves on lymph transport shedding light into some of the potentially underlying consequences of lymphedema. Polyethylene glycol (PEG) coated latex particles were injected into the inguinal lymph node of anesthetized mice. Particle displacement measurements through efferent lymphatic vessels yielded velocity, wall shear stress, vorticity and strain of the efferent lymph flow field carrying lymph from subdermal inguinal lymph nodes. Lymphatic vessel endothelial Prox1 green fluorescent protein (GFP) marker enabled the detection of lymphatic vessel walls and valves. Flow field, flow velocity, flow rate, velocity profiles, wall shear stress, vorticity and strain values were compared in regions downstream of normal and malformed valves in two wild type mice. A Clec2-deficient mouse, which experiences lymphatic development defects and is used as a lymphedema model, was employed to further elucidate the lymphatic valves on transport.

The absence of centralized pumping yields highly variable lymphatic flow cycles varying from one to fifteen seconds. The presence of lymphatic valves introduces boundary conditions that yield spatial and temporal flow gradients increasing the degree of complexity of lymph transport. The valves dictate the trajectory of the particles and promote the formation of recirculation zones. Even in the presence of valves, lymph flow commonly reverses. Congenital defects like a single leaflet valve lowers the lymph flow efficiency and promotes higher wall shear stress regions. Furthermore, the absence of

functional valves in the Clec2-deficient mouse not displaying lymphedema yielded lymph flow lacking the pulsatility that characterizes normal lymphatic flow.

TABLE OF CONTENTS

Page

LIST OF TABLES

Table **Page**

LIST OF FIGURES

Figure **Page**

CHAPTER 1

INTRODUCTION AND BACKGROUND

1.1 The Lymphatic System

The circulatory system is comprised of two separate systems: the cardiovascular system, which distributes blood, and the lymphatic system, which circulates lymph. The blood circulatory system is a closed system, whereas the lymphatic system is one-way open system.

Arterial blood carries oxygen, nutrients, and hormones for the cells. Oxygenated blood travels arteries, arterioles and capillaries to perfuse tissues throughout the body. During this process fluid, primarily plasma, travels between cells as interstitial fluid and it delivers its nourishing products to the cells. This fluid along with cellular waste is transported via the lymphatic system into the venous system.

One of the primary roles of the lymphatic system is to transport this excess interstitial fluid back to the blood circulation via the thoracic duct into the venous system [1], [2]. Along with the excess interstitial fluid, excessive proteins and waste are transported back to the circulation. The lymphatic system also acts as a conduit for immune cells and facilitates the immune response. Lymph nodes across the network filter the interstitial flow and provide immunity against bacteria, viruses and waste. Thus, along with being an integral part of the circulatory system, the lymphatic system is also an integral part of the immune system.

1.1.1 Anatomy and Physiology

Unlike the cardiovascular system, the lymphatics do not have a centralized pumping organ. The lymphatic system is composed of a network of vessels, termed as lymphatics, lymph nodes and lymphoid organs. Anatomically, the vessels of the lymphatic system are sub-divided into the initial lymphatics, pre-collecting lymphatics, collecting lymphatics and organs such as nodes. The origins of the lymphatic system, known as the initial lymphatics, are dispersed throughout the capillary network of the mesentery. The walls of the initial lymphatics are usually not contractile and only lined with endothelial cells.

All tissues connected perfused by the cardiovascular system have supporting lymphatics to serve as its drainage system, with the notable exception of bone marrow and the central nervous system [3]. Lymphatic capillaries are tiny, thin-walled blind-ended vessels composed of a single monolayer of non-fenestrated lymphatic endothelial cells (LEC) and are present in all tissues in the interstitial spaces [4]. The lymphatic capillaries are strategically placed and anatomically constructed to permit a continuous and rapid removal of transient interstitial fluids and plasma proteins from the interstitium. The endothelial cells are arranged in an overlapping pattern and each cell is attached to nearby tissue by anchoring filaments to keep them from collapsing under higher fluid pressures [5]. The anchoring filaments are mainly composed of the emilin-1 and fibrillin proteins, which may attach to the LECs via molecules such as αvβ3 integrin [6], [7]. When pressure in the interstitium is greater than in the capillaries, the flap-like endothelial cells separate slightly and interstitial fluid enters the lymphatic capillary. In contrast, if pressure is greater inside the lymphatic capillary, the LECs adhere closely, to prevent retrograde flow. The fluid entered in the capillaries is now termed as lymph

which is a clear fluid with an approximate density of 1000 kgm^{-3} [8] and the dynamic viscosity ranging between 1.5×10^{-3} and 2.2×10^{-3} cP [9].

The lymph travels from the capillaries into the pre-collecting lymphatics. The pre-collecting lymphatics connect the lymphatic capillaries to the collecting vessels. They contain bicuspid one-way valves; however, the distribution of valves is irregular and even comprise occasional single leaflet valves [10]. Smooth muscle cells are observed in the pre-collecting and larger lymphatic vessels. The presence of smooth muscle cells decreases vessel permeability in these vessels, while its absence enables fluid adsorption in the initial lymphatics.

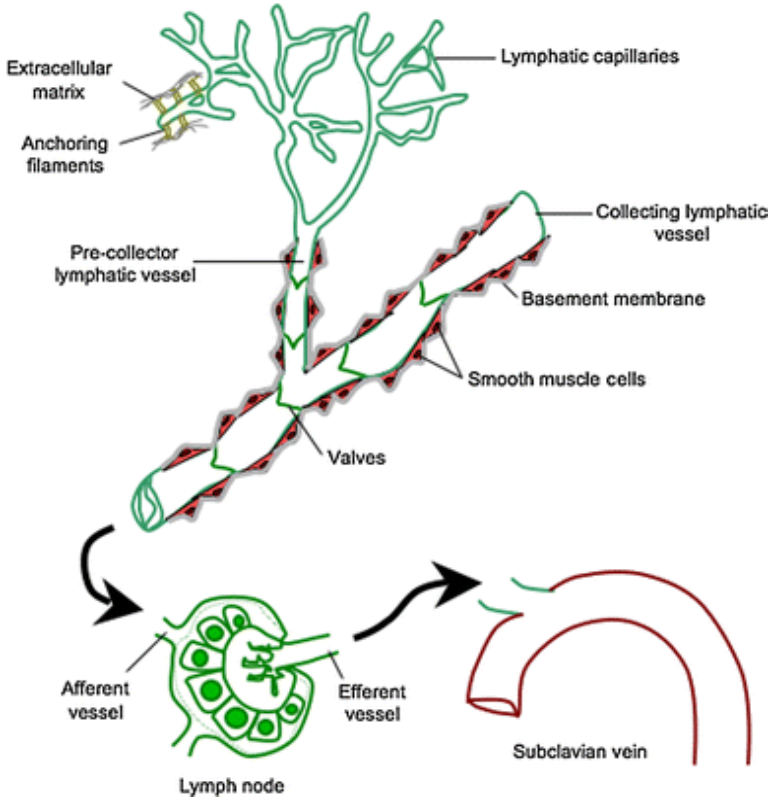

Figure 1: Organization of lymphatic vascular system [7]

The collecting lymphatics deliver lymphatic fluid to the lymph nodes through afferent vessels and drain the lymph away from the node through efferent lymph vessels. The collecting lymphatic vessels connect with chains of lymph nodes that sieve and monitor lymph to mount an immune response when necessary. The collecting lymphatics differ from the capillaries and pre-collector vessels, especially in lumen diameter. Intraluminal lymphatic valves are present primarily to ensure net antegrade flow. The part of the vessel between two valves is known as a lymphangion. The lymphatics is composed of a series of connected lymphangions.

Lymph propulsion is the outcome of contractions of the lymphangions and by external motion of skeletal muscle, arteries and veins. In this manner, the lymph is transported by pumping towards the venous system in the neck region [2]. Lymph from the left side of the body, abdomen, and both lower limbs ends up in the thoracic duct, the largest lymphatic vessel that runs alongside the aorta, and finally connects with the left subclavian vein. Lymph from the right upper arm, thorax, and head is returned to the right subclavian vein via the right lymphatic trunk [11]. In healthy adult individuals, the lymphatic system returns as much as eight liters of interstitial fluid with 20–30 g of protein per liter to the venous circulation every day [3]. The wall structure of these vessels are similar to that of blood vessels and consists of three layers: the intima, media and adventitia [12].

1. **Intima:** The inner layer of lymphatic vessels is composed of a single monolayer of lymphatic endothelial cells (LEC), also known as the lymphatic endothelium. The lymph is in direct contact with the endothelial cells. Lymphatic endothelium is further discussed in detail in next sub-section.

2. **Media:** Smooth muscle cells are arranged in a circular fashion around the endothelium that help alter the lumen pressure by contracting and relaxing. The activity of smooth muscles allows lymph vessels to slowly pump lymph fluid through the body. Smooth muscle cells are absent in initial lymphatics. An extensible protein called elastin enables reshaping of the vessel after contraction.
3. **Adventitia:** The outermost layer of the vessel is the adventitia, consisting of fibrous tissue. It is primarily composed of collagen and serves to anchor the lymph vessels to structures within the body for stability. Larger lymph vessels have many more layers of adventitia than the smaller lymphatic vessels. Adventitia is absent in initial and pre-collecting lymphatics.

The lymphatic vessels are comparable to blood vessels, however, structure of smooth muscle, elastin and collagen networks in the lymphatic walls are not present in blood vessels [13]. Blood vessel walls are not designed to contract spontaneously, since the heart pumps the blood around the body. Blood vessels experience mainly radial stresses [13]. The lymphatic walls actively pump the lymph which creates longitudinal as well as radial stresses. The forces present in the cardiovascular system are much higher than in the lymphatic system. Additionally, as the velocities in the lymphatic system are much slower, the Reynolds numbers are significantly lower than in the cardiovascular system.

1.1.2 Lymphatic Endothelium

Lymphatic endothelial cells (LECs) originate from embryonic blood endothelial cells (BECs) during embryogenesis. The hematopoietic signalling proteins SLP76 and SYK are known to regulate blood and lymphatic vascular differentiation during development [14]. The two endothelial cell types, therefore, share features such as flat morphology, apico-basal polarity and certain common endothelial-specific proteins. However, many phenotypic and genetic characteristics are unique for one or the other vessel type and are routinely used to differentiate between blood and lymph vessels in histological specimens and vascular biology. Recent studies have demonstrated that the BECs and LECs represent differentiated cell lineages without evidence of any interconversion between the distinguishing phenotypic properties [15].

The LECs are terminally differentiated cells distinct from blood vascular endothelial cells [16]. This has enabled the discovery of lymphatic vascular-specific molecules that are used for identification of lymphatic vessels in tissues, as well as for finding targets for the specific induction or inhibition of lymphatic vessel growth in pathological conditions [16], [17]. Blood vessels express plasmalemma vesicle associated protein 1 (PV-1), endoglin, neuropilin-1 (NRP-1) and collagen IV [18]. Lymph vessels on the other hand express markers such as podoplanin (PDPN), lymphatic endothelial hyaluronan receptor-1 (LYVE-1) [19], vascular endothelial growth factor receptor-3 (VEGFR-3) and prospero related homeobox 1 (PROX-1) [18]. Among these, the transcription factor PROX-1 is known to be the most specific lineage marker for LECs [20] and for the downregulation of numerous BEC-specific genes [21]. LYVE-1

expression remains high in lymphatic capillaries and decreases in collecting lymphatic vessels [22].

ECs that line the lumen of blood and lymphatic vessels are exposed to mechanical forces generated by fluid flow. The endothelium responds to shear stress through various mechanosensitive pathways depending on the kind and the magnitude of shear stresses (9). LECs exposed to shear stresses due to flow have shown upregulation in genes such as FOXC2, GATA2, ITGA9 and CX37 during development and promote valve formation [23]. PROX-1expression is not altered by lymphatic fluid shear forces. LYVE-1 expression is significantly downregulated.

Modulating shear stress through flow rate has been found to induce release of the vasodilator nitric oxide (NO) in lymphatic vessels. As in blood vessels, the SMCs lining the lymphatic vessels respond to changes in Ca^{2+} concentration, which generally alter vessel contraction [24], [25]. NO acts at multiple points in the Ca^{2+} contraction pathway to modulate Ca^{2+} release and uptake, as well as the enzymes responsible for force production [26], [27]. Blocking or enhancing NO activity can dramatically affect pumping behavior. Studies have investigated and revealed that NO release is driven by upregulation of enzyme endothelial nitric oxide synthase (eNOS) in LECs. NO produced by eNOS in the vascular endothelium plays crucial roles in regulating vascular tone and cellular proliferation. Another study has revealed the role of shear stress in phosphorylation of eNOS, thus upregulating NO [28] .

1.1.3 Lymphatic Valves

One of the main structural features of lymphatic vessels are their valves, which are normally semilunar structures attached to opposite sides of the lymphatic endothelium. Valves are present even in the blood circulatory system, but only in low pressure venous circulation. They function similarly to lymphatic valves, however are more dependent on skeletal muscle contractions. Lymphatic valves are found in larger lymph vessels and collecting vessels and are absent in the initial lymphatics. The valves serve to prevent retrograde flow during relaxation of the vessel wall and to promote net forward flow [29]. Ideally, the pressure of lymph increases to a certain point due to lymph volume or from smooth muscle contraction, the fluid will be pushed through the valve into the next chamber of the vessel, lymphangion. As the pressure drops, the open valve then closes so that the lymph fluid cannot flow backwards.

Lymphatic valves are composed of 2 intraluminal leaflets, each of which is formed by two layers of LECs separated by an extracellular matrix–rich core [30]. Generally, the lymphatic valves are of the bicuspid type, regardless of the species [31]. However, up to five leaflet valves as well as single leaflet ones have been observed. Studies have shown that smooth muscle cells (SMC) are absent from the valve leaflets [8]. The lymphangions, thus, do not have the ability to contract in the valvular regions due to absence of SMCs.

Studies have shown defects in valve formation due to certain genes such as FOXC-2 and lymph flow during development. Valvular malformations can promote lymphatic system dysfunctions which are discussed in detail in the next section [32].

1.2 Lymphatic System Malfunction

Abnormal function of lymphatic vessels is important in multiple diseases including inflammation and cancer. The lymphatic vessels contribute to a wide range of human diseases such as inflammation, lymphatic insufficiency, obesity, hypertension and metastasis platform for tumors [3]. Impaired lymphatic function, reduced numbers of lymphatic vessels and valvular insufficiencies cause disruption of lymph transport [33]. The outcome of a disrupted lymphatic system is compromised lymph drainage. The lymph is retained in the vessels and the interstitial sites, the ability to maintain fluid balance and tissue homeostasis is compromised and immune function can be impaired. This condition is one of the most common forms of lymphatic dysfunction and is coined lymphedema.

The two major classifications of lymphedema are primary and secondary [34]. Primary lymphedema can be genetic or congenital and can be first noticed birth or it can develop later in life during puberty or later. Unlike primary lymphedema, secondary lymphedema is caused due to damage to collecting lymphatic vessels.

Although primary lymphedema is a rare condition, identification of the underlying genetic causes has provided insight into the molecular mechanisms regulating the development and function of the lymphatic vasculature. Insights into the molecular and genetic mechanisms of lymphedema have been greatly enhanced over the last few years [20]. This is mainly attributable to:

(1) the discovery of gene mutations in two different types of lymphedema,

(2) the identification of specific receptors on LECs

(3) the recent development of genetic mouse models for cutaneous lymphedema.

Two lymphangiogenic factors, VEGF-C and VEGF-D, and their lymphatic receptor VEGFR3 gene have been identified as a major cause of Milroy disease, which causes lymphedema due to hypoplasia of lymphatic capillaries and is typically observed at birth [3]. Primary lymphedema has been classified as Milroy disease when present at birth (Milroy 1892), or as Meige disease, which develops predominantly after puberty (Meige 1898). Both diseases are characterized by a combination of dilated lymphatic capillaries and interstitial accumulation of lymph fluid leading to lymphedema. Mutations in the transcription factor FOXC2 have been linked to lymphedema-distichiasis (LD) characterized by late-onset lymphedema and varicose veins [35]. Previous studies of FOXC2 mutant mice reveals that LD is due to loss of valves in the collecting vessels. Similar results are observed in samples obtained from LD patients [21]. Heterozygous missense mutations in α9 integrin (ITGA9) underlie congenital chylothorax in human fetuses, recapitulating the results obtained by gene targeting in mice [36].

Dominant-negative mutations of the homeobox transcription factor SOX18 have been linked with hypotrichosis-lymphedema-telangiectasia syndrome [37]. Mutations in the NF-κB regulatory protein NEMO associate with a rare and complex syndrome involving lymphedema [38] .

C-type lectin–like receptor 2 (CLEC2) deficiency in mice develop normal lymphatic system, but the lymph flow is opposed by the backflow of blood from the venous system as the result of a hemostatic defect [39]. C-type lectin–like receptor 2 (CLEC2) is a cell-surface receptor and is expressed by platelets. Previous studies have reported the presence of lymph flow playing a central and broad role in the development of collecting lymphatic vessels and valves [23]. CLEC2-deficient animals with reduced

lymph flow, thus, lack lymphatic valves, fail to remodel the primitive mesenteric lymphatic plexus into a hierarchical collecting vessel network, and exhibit premature and excess smooth muscle cell coverage of their collecting lymphatic vessels. CLEC2-deficient mice can thus be used as lymphedema models [23].

Secondary lymphedema is acquired due to damage to the lymphatic vessels due to surgery or from lymphatic filariasis [40], caused by a parasitic worm invading the lymphatic system. Filariasis causes a complete and permanent disruption of lymphatic transport, resulting in chronic lymphedema of the legs and genitals [41]. The onset of filariasis is triggered by a filarial-specific inflammatory reaction that promotes the production of VEGF, VEGF-C, and VEGF-D, which leads to persistent hyperplasia of the lymphatic vessels [42]. Filariasis is the principal cause of lymphedema worldwide, affecting approximately 100 million people [42]. Arm lymphedema is very common in breast cancer patients as an outcome of node dissection during surgery [8].

Lymphedema is progressive and lifelong and very few treatments have been proposed to restore flow and resolve the lymphedema. The treatment of lymphedema is currently based on physiotherapy, compression garments, liposuction, and occasionally surgery for manual lymphatic drainage, however, the longevity of the treatment is unknown [43].

1.3 Vascular Fluid Dynamics

The Reynolds number, *Re*, is the ratio of the inertial fluid forces to viscous fluid forces. At lower values of Reynolds number, the viscous forces dominate the fluid flow. It has been noted that the Reynolds number in the collecting lymphatics is small due to

the viscosity of the flow and the size of the vessels [44]. It has been assumed that lymph is a Newtonian fluid and does not contain solid particles [45], [46]. In Newtonian fluids, the viscous stresses are proportional to the local strain rate,

$$\dot{\gamma} = du/dr$$

where μ is the kinematic viscosity of the fluid, *u* is the tangential velocity component and *r* is the radial spatial variable. Newton's law for shear stress is given by:

$$WSS = \mu * \dot{\gamma}$$

$$WSS = \mu * \frac{du}{dr}$$

Normal stresses due to fluid pressure are transferred to all vessel wall layers (intima, media and adventitia). In contrast, shear stress is experienced by the cellular inner layer, endothelium, in contact with the flowing fluid.

1.4 Objectives

Despite the importance of the lymphatic system in health and disease, it remains overlooked in terms of research, especially compared with the blood circulatory system [48], [49]. The study of the lymphatic system is still in its infancy. Studies of the uptake and transport of drugs into the body via the intestinal lymphatic system have received increasing attention in recent years. The effective transport of fluid in the lymphatic system is important for preventing consequences such as lymphedema. It is essential that we understand how various lymphatic diseases alter the vessel mechanical environment. Improving our understanding of lymph fluid flow will enhance our knowledge on how

lymphatic transport of waste, immune cells, and proteins around the body and potentially develop new ways of treating lymphedema by understanding the origins of the disease. The primary objective of this study is to compare the effects of single leaflet valve malformation in wild type mouse to normal valves within the same animal as well as in other wild type mouse. The single leaflet valve is hypothesized to affect the flow and thus, effective lymph transport. This mouse serves as a model to study valvular insufficiency and malformations that can potentially contribute to lymphedema.

Biological processes involving endothelial cells are often studied *in vitro* due to the challenging nature of *in vivo* studies. However, characterizing the flow field experienced by LECs *in vivo* is key to understanding how the lymphatic system functions in normal and disease states.

One example where lymph fluid dynamics may be important is in cancer metastasis. The lymphatic system is the metastatic route for various types of cancers. Metastasis through lymphatic system is recognized to precede hematological spread in many cancers including melanoma, breast, colon, lung and prostate cancers. The lymphatics, thus, have the potential to play a large role in anticancer treatment [47].

CHAPTER 2

EXPERIMENTAL SETUP

2.1 Experimental Summary

Four mice were anaesthetized using 2,2,2-Tribromoethanol (Sigma-Aldrich) dissolved in tert-amyl alcohol (Sigma-Aldrich) (0.5 mg/g), and body temperature was maintained at 37°C throughout experiment [23]. Ventral skin was peeled back to expose an inguinal lymph node. The inguinal lymph nodes are located medial to the femoral vein and under the cribriform fascia as shown in Figure 2.

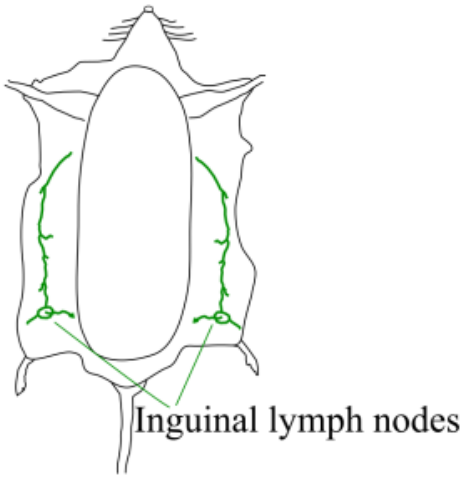

Figure 2: Anaesthetized mouse with ventral skin peeled back exposing the inguinal lymphatic nodes

Because the lymphatic network is filled from the periphery, it is difficult to globally label lymph, thus, fluorescent particles were introduced in the lymphatics. The inguinal lymph node was injected with 5 µl of FluoSpheres (1 µm beads, 580/605, Invitrogen) diluted in sterile PBS for a concentration of 1×10^8 beads/ml. The beads were

coated with Polyethylene Glycol (PEG), a hydrophilic molecule, to avoid binding of particles to each other and to the vessel.

The efferent (post-nodal) lymphatic vessel was imaged for several minutes immediately following bead injection under a dissecting microscope as shown in Figure 3. Lymphatic endothelial PROX1 green fluorescent protein (GFP) marker enabled lymphatic vessel edge detection.

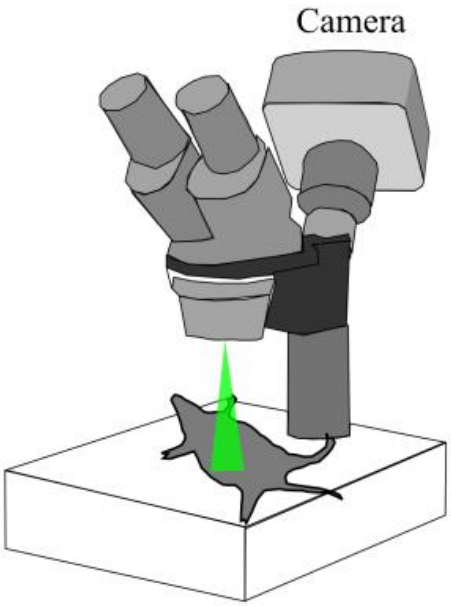

Figure 3: Anaesthetized mouse under a dissecting microscope. The efferent vessel to inguinal lymphatic node was imaged.

2.2 Image Acquisition

Fluorescent-based imaging techniques are commonly implemented in animal research to overcome the poor contrast that is often inherent in biological imaging. Live animal imaging was conducted as shown in Figure 3 using green and red fluorescence and an Olympus MVX10 dissecting microscope. The mice employed expressed PROX1 green fluorescent protein in LECs. In contrast, the injected particle tracers fluoresced red. Particle displacement through efferent lymphatic vessels was imaged for several minutes. One of the primary challenges in imaging was the animal moving the plane of interest in and out of focus due to breathing and other muscular movements.

2.3 Mice Specifications

Two four-week-old wild type mice were considered for the studying the effects of single leaflet valve. Additional mouse cases involving a wild type mouse and a *Clec2*$^{-/-}$ Mouse were imaged for further studies. The phenotype of each mouse is described in Table 1. The weights of the mice varied from 14 to 25 grams.

Table 1: Mice specifications. Mouse 1 (control) and Mouse 2 were considered for the study

Case	*Phenotype*	*Valves*	*Abbr.*
MOUSE 1	Wild-Type	One normal bi-leaflet valve	WT
MOUSE 2	Wild-Type	Two bi-leaflet valves, One uni-leaflet malformed valve	MV
MOUSE 3	Wild-Type	One normal bi-leaflet valve	WT2
MOUSE 4	Clec2-Deficient	Abnormal non-functional valve	$Clec2^{-/-}$

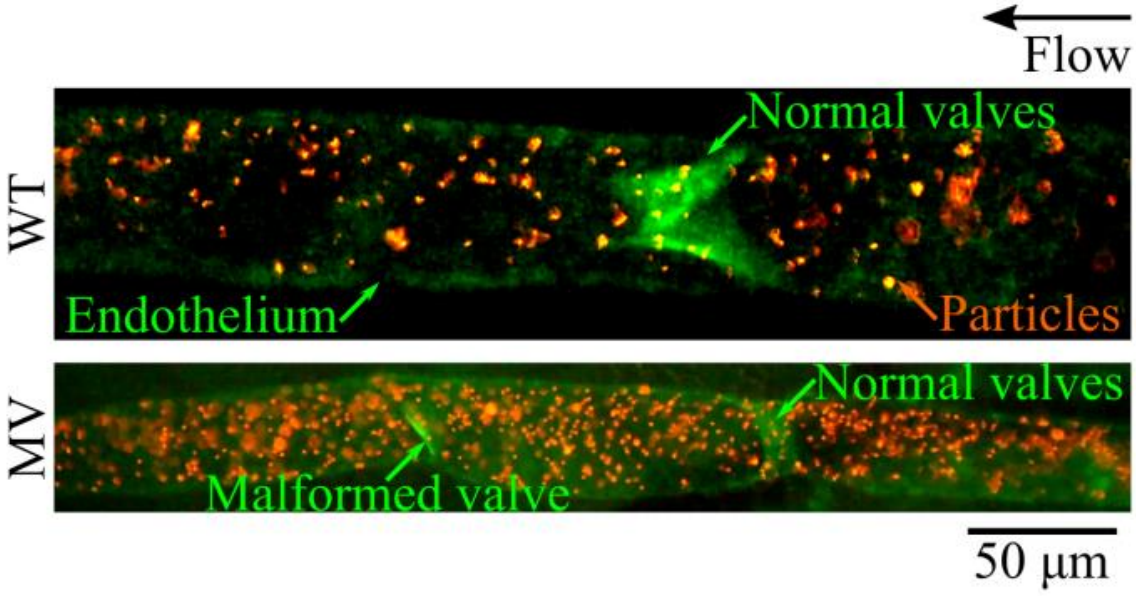

Figure 4: Image acquired from WT Mouse and MV Mouse. The green fluorescence depicts the labeling of the lymphatic endothelium by PROX-1 GFP. The particles stained in red dye are seen in red.

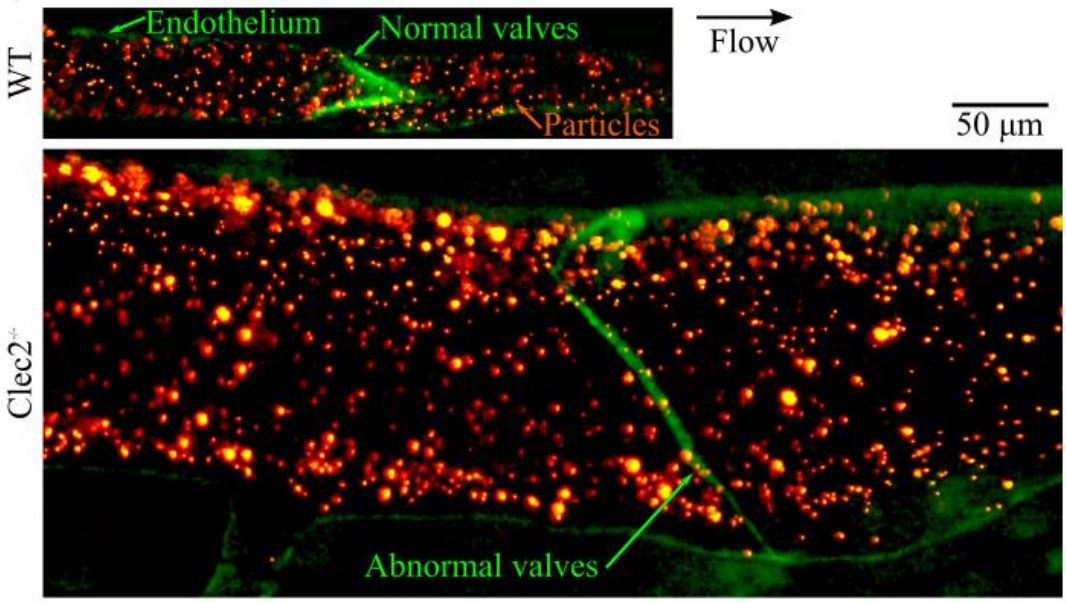

Figure 5: Image acquired from WT2 Mouse and *Clec2*$^{-/-}$ Mouse. The green fluorescence depicts the labeling of the lymphatic endothelium by PROX-1 GFP. The particles stained in red dye are seen in red.

Table 2: Mice image specifications

Case	*Image Size (pixels)*	*Image Size (µm)*	*Frame Rate (fps)*	*Flow Direction*
MOUSE 1	1301 × 305	361 × 85	30	Right to Left
MOUSE 2	1391 × 181	386 × 50	30	Right to Left
MOUSE 3	1181 × 246	328 × 68	30	Left to Right
MOUSE 4	1911 × 841	530 × 233	30	Left to Right

2.4 Immunohistochemistry Experiments

Based on few previous studies and as discussed in the previous chapter, eNOS was found be upregulated in the LECs subjected to higher flow. It was hypothesized that the region downstream of valves would be subjected to higher flow velocities and higher WSS. To verify this hypothesis, immunohistochemistry (IHC) experiments were performed on mouse tissues to study the expression of eNOS in the lymphatics.

IHC was performed on mesenteric gut acquired from 3 to 10 days old wild-type (WT) mice. Greater adipose tissue in the mesentery of older animals increases the degree of complexity when imaging the lymphatics, thus mice younger than 10 days were selected. Mesenteric gut was dissected carefully from mice, thus, preserving the morphology and the lymphatics surrounding the mesentery. All samples were washed three times with PBS (Life Technologies) and fixed with 5% formalin (Fisher). The tissues were then washed with PBS along with 0.1% Triton-X (Sigma-Aldrich) (PBS-Tx) to promote permeabilization. To minimize nonspecific binding of the primary and secondary antibodies, blocking solution casein (Life Technologies) was used for 30-min at room temperature followed by adding primary antibodies eNOS (Santa-Cruz Biotechnology) and PROX1 (Abcam) diluted 1:120 in blocking solution. The tissues were then incubated overnight at 4-degree Celsius. This was followed by three washes in PBS-Tx and overnight incubation with the secondary antibodies that were fluorescently tagged - Alexa Fluor 488 chicken anti-goat (Life Technologies), diluted 1:250; Alexa Fluor 488 donkey anti rabbit (Life Technologies), diluted 1:250. The samples were then washed with PBS-Tx in a dark room to avoid photobleaching. The gut was then carefully emptied using forceps to remove partially digested food which is auto-fluorescent under a

dissecting microscope in a dark room. Smaller samples of tissues were mounted on glass slides using vectashield mounting media (Sigma-Aldrich) and cover slips, and examined with a confocal microscope. Imaging was performed at 20x and PROX1-GFP enabled the detection of lymphatics.

CHAPTER 3

ANALYSIS METHODS

3.1 Image Processing

Particle displacement through efferent lymphatic vessels was imaged with a dissecting microscope as discussed in Chapter 2. Twenty-five seconds of data were selected from each recording with 30 frames per second imaging a single plane for a total of 750 fluorescent images.

A custom denoising program was written for detecting and removing artifacts and stabilizing images affected by breathing of the animal, muscle activity, amongst other causes. The first image in the series served as the reference image to stabilize all other images in the series. First, all images were cross-correlated with the first image to obtain a coarse displacement for each image with relation to the first image in the series. The coarse displacement data was then used to align the images with respect to the first image in the series. A finer image displacement calculation was conducted using the stabilized series and the Template Matching and Slice Alignment ImageJ Plugin. A third run was conducted in MATLAB incorporating the two separate displacement datasets. With these displacement datasets, the power spectral density was calculated revealing the power present in the signal. Peaks in the signal coincide with animal breathing rate, muscle twitching and other physiologically related movements (Figure 6 and Figure 7).

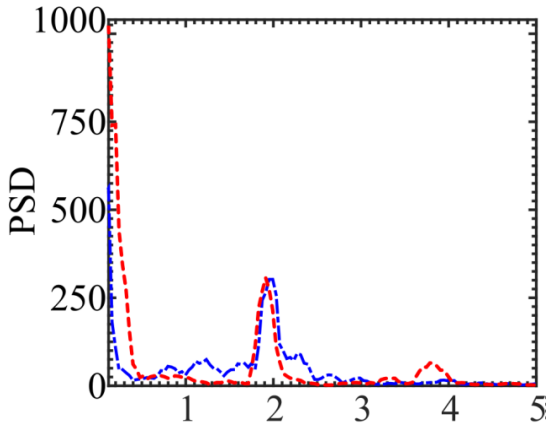

Figure 6: Power Spectrum Density for the WT Mouse (Blue) and MV Mouse (Red)

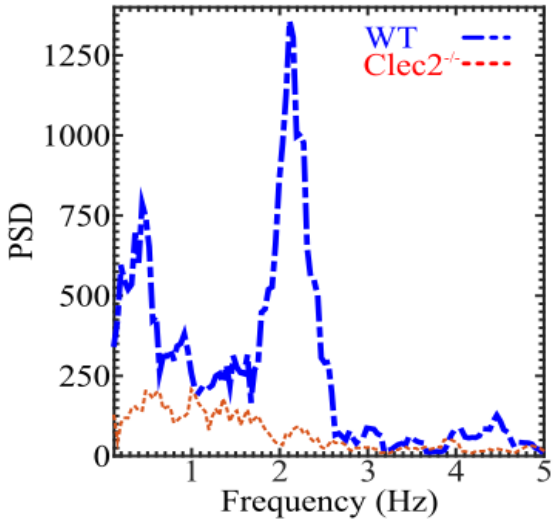

Figure 7: Power Spectrum Density for WT2 Mouse (Blue) and *Clec2*$^{-/-}$ Mouse (Red)

ImageJ (National Institutes of Health, Bethesda, MD) and MATLAB (MathWorks, Natick, MA) were used for post processing to retrieve data from images post hoc such as vessel diameter, particle velocity, etc. as discussed in subsequent sections.

3.2 Vessel Edge Detection

We define the process of partitioning an image into multiple segments of pixels as image segmentation. All the pixels in a region are similar with respect to some characteristic or computed property, such as color, intensity, or texture. These objects can be processed or analyzed for the extraction of quantitative information. Live animal data can be noisy and consequently difficult to segment accurately.

Edge detection includes a variety of mathematical methods that aim at identifying points in an image at which the image brightness changes sharply or has discontinuities. The points at which image brightness changes sharply are typically organized into a set of curved line segments termed edges. The discontinuities in an image are found by calculating the first and/or second order derivatives of an image. A multi-step algorithm – Canny-Deriche edge detector [48] was implemented to identify the set of bright pixels from the green channel representing the vessel edge. The green channel in the images corresponded to the expression of endothelial Prox1-GFP.

The pixels representing vessel edge were detected by Canny-Deriche algorithm and were stored in file for each frame for each of the mouse cases. Each pixel had an x and y coordinate value. The number of pixels stored was dependent on the brightness of the edge and clarity of the image. Lesser number of pixels were stored for out of focus frames.

MATLAB was used to analyze the pixel data. A local regression technique was implemented to identify the vessel edge curve. The local curve fitting technique helps identify accurately the shape of the vessel. However, the fitting varied in successive frames. To account for sudden changes in the vessel geometry in successive frames,

spatial and temporal smoothing was performed on the fitted curves. Each frame now had two sets of x and y coordinates which represented the top and bottom curves of the lymphatic vessel (Figure 8).

The vessel diameter was calculated as the distance between top and bottom curves of the vessel after considering the angle of orientation of the lymphangion. The diameter, D, was computed at every point of the vessel for all the frames.

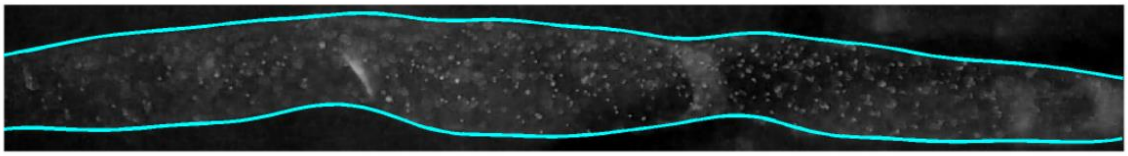

Figure 8: Curves showing the outcome of edge detection procedure on a green channel image for MV Mouse case

3.3 Particle Tracking

Particle tracking velocimetry is a technique to measure velocity of particles that are resident in a fluid. This technique is based on Lagrangian approach which involves tracking individual particles. The local particle tracking is based on comparison of successive frames. To calculate the individual particle shift, sub-regions much smaller than the images are analysed from two different successive images acquired Δt time apart within that specific interrogation window area.

Several computational tools are available to assist with detection of shapes or particles and to evaluate the trajectories of the identified shapes in a sequence of images. Particle tracking tools assume the target particles to be brighter than the local background. Image quality and frame rate significantly affect the results of automated

particle tracking. Higher frame rate values ensure the distance travelled by a particle is lower between the frames.

3.3.1 Challenges

A major challenge of particle tracking is the fact that segmented objects at different time points may have no relationship between consecutive frames. The steps for successful tracking are:

(i) To correctly identify the objects that should be part of the same track.

(ii) To accurately join them as part of a track.

(iii) To precisely track the objects position even if on occasion the object may disappear or reappear.

The detection of particles *in vivo* in a two-dimensional focal plane makes particle tracking complex because the breathing of the animals renders the plane of interest out of focus and blurry. Computationally, blurry particles are labelled as particles with larger diameters. Thus, particle tracking tools fail to identify a particle in subsequent frames if it changes in size and brightness and the software assigns different labels to the same particle in different frames. Particle density and clustering of particles present further challenges in unique particle identification. Also, some particles closer to the vessel wall tend to be stationary, while particles away from the wall flow over the stationary particles.

3.3.2 Tracking Tools Used

ImarisTrack (Bitplane, Belfast, UK) software for two-dimensional images was used for initial particle detection and tracking (Figure 9). Due to computer RAM limitations, entire sequence of images could not be imported into the software and the image sets were into shorter image sequences. Statistical data such as particle coordinates, track identification number, span of the tracks was extracted from ImarisTrack. A custom MATLAB code was written to combine entire tracking data by merging tracks for each mouse case.

However, due to challenges in tracking as discussed previously, the tracking of particles was not accurate. Particle coordinates from ImarisTrack were converted to .mdf files that could be read by the MTrackJ plugin for ImageJ. The MTrackJ plugin offered greater manual control for manual tracking and was used for interactive manual trajectory inspection, modification and creation.

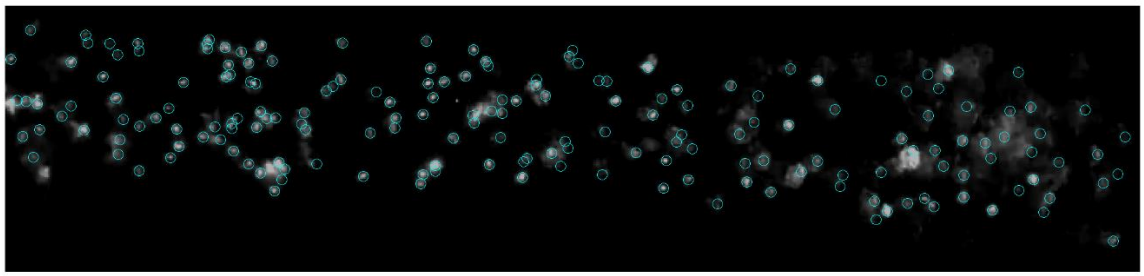

Figure 9: Sample image depicting the location of detected particles in a frame in the WT Mouse

3.3.3 Particle Velocity

A unique identification number was allotted to each particle after manual tracking was performed in mTrackJ. The velocity of the particle was computed using the particle coordinates from two consecutive frames and calculate as follows.

$$u_t = \Delta x/\Delta t$$

$$v_t = \Delta y/\Delta t$$

Based on directionality of the flow of the particles, the sign convention was defined for each case (Table 3). Forward flow depicts the flow of lymph moving towards veins from the interstitium.

Table 3: Velocity sign convention

Forward moving particle	positive	+ u
Backward moving particle	negative	- u
Upward moving particle	positive	+ v
Downward moving particle	negative	- v

3.4 Region of Interests

Presence of valves and lack of pumping organ promote variable flow fields in the lymphatics. Retrograde flow adds to the degree of complexity within the flow. The flow fields vary temporally within a single lymphangion as well. In order to compare lymphatic fluid flow within different regions of the lymphatic vessels, segments of equal width were defined at different regions of the vessels as shown in Figure 10 and Figure 11. Figure 10 is for the control mouse with a single bi-leaflet valve (WT) and Figure 11

for a mouse with one uni-leaflet and two bi-leaflet (MV). Since SMCs are present around each lymphangion, it is expected that the vessel contraction is maximum at the center of the lymphangions. Hence, the center was defined based on the maximum contraction of the vessel within that lymphangion. The distance of the segment downstream from the valves was kept at a constant ratio based on the length of the lymphangion. Fluid and vessel properties were analyzed in the defined segments.

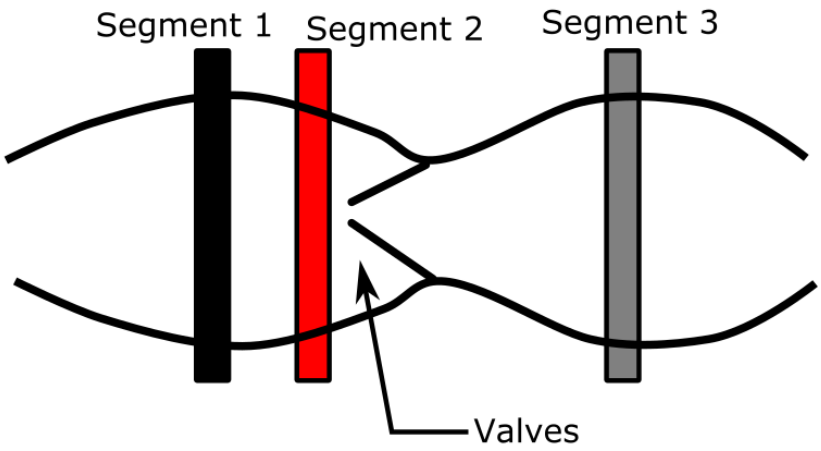

Figure 10: Defined segments in WT Mouse

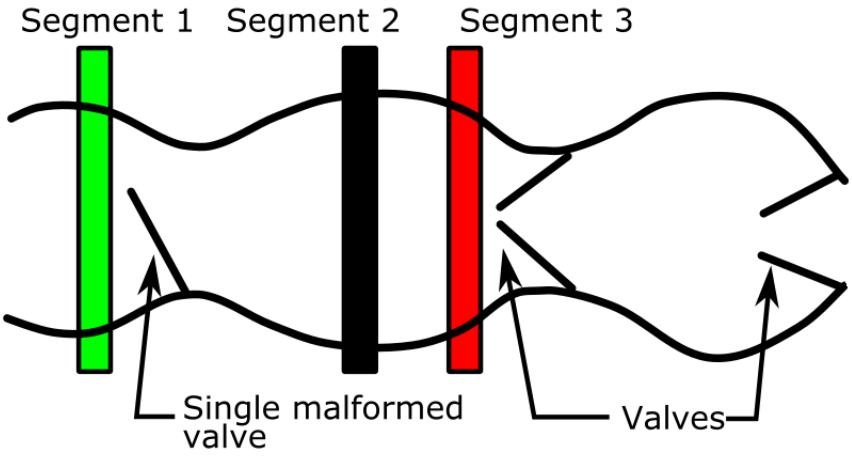

Figure 11: Defined segments in MV Mouse

3.5 Particle Data Interpolation

The number of particles flowing inside the vessel varied for each mouse case. Hence, a custom function was generated to interpolate the particle displacement in order to generate a uniformly distributed vector field. Zero velocity no-slip condition was considered at the vessel wall and valve surfaces. MATLAB function *griddata* for two-dimensional non-uniformly spaced was used to interpolate the values of velocity components on a gridded mesh. Triangulation-based cubic interpolation method was implemented [49] for second order continuity.

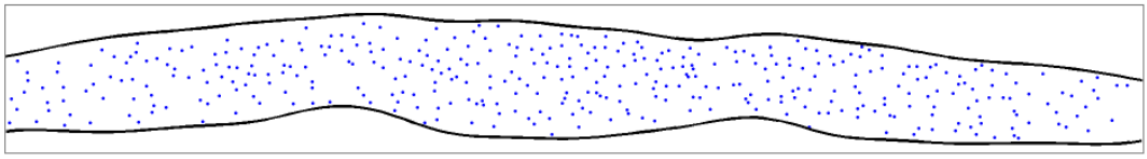

Figure 12: Location of actual particles in MV Mouse at a random time point

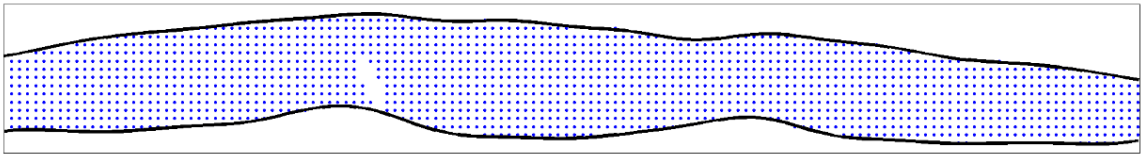

Figure 13: Interpolated pseudo-particles in same frame in MV Mouse

Figure 12 shows the coordinates (x, y) of actual particles at an instant within the Mouse 2 vessel and Figure 13 shows the uniformly space coordinates inside the vessel. The values of velocity, vorticity, shear strain and normal strain were then calculated at all points in the interpolated data.

CHAPTER 4

RESULTS AND DISCUSSION

4.1 Overview

The data presented in this chapter are results after image analysis for two mice. WT Mouse and MV Mouse were used to study the effects of valve malformation. The comparison of valves or regions was based on calculations in segments defined in section 3.4. Vessel contraction, fluid velocity, development of velocity profiles within a flow cycle, variable trajectory of particles, flow fields changes within a flow cycle, wall shear stress, vorticity and strain were calculated and compared. A lymphatic universal flow function is proposed.

4.2 Vessel Contraction Over Time

Differences in vessel diameter were observed in each animal. The value of diameter changed from lymphangion to lymphangion within the same animal as well. Due to heterogeneity in vessel size and, normalization techniques were implemented for comparison of parameters in different animals.

Figure 14 shows the movement of vessel or the change in vessel diameter at defined segments in WT Mouse and MV Mouse. Vessel diameter is expressed in terms of non-dimensional diameter (D/D_{max}), wherein $D/D_{max} = 1$, represents the maximum vessel diameter in that particular segment. Maximum vessel diameter implies vessel in dilated form and smaller values indicate contracted vessel due to the SMCs and other factors. Elastin helps contracted vessel to retain its shape.

In diameter analysis of WT and MV Mice cases, the maximum contraction was observed at the center of the lymphangion and no contraction was observed in the valvular regions. This confirms that the absence of SMCs yield no vessel contraction.in the valve region of collecting lymphatics. However, the contraction at the center segment of the lymphangions is greatest (Figure 14a) for WT Mouse, wherein gray and black curves depict center of two neighboring lymphangions. The segment immediately downstream of the uni-leaflet valve was found to contract less in comparison to the segment downstream of bi-leaflet valve in MV Mouse (Figure 14b).

The contraction pattern observed in three cases was different and no correlation was found in the correlation study. The maximum vessel contraction observed was approximately 9% and 16 % in WT and MV, respectively. The contraction differences in comparison to different cases and even within the same animal in different lymphangions shows the heterogeneity of the lymphatic system.

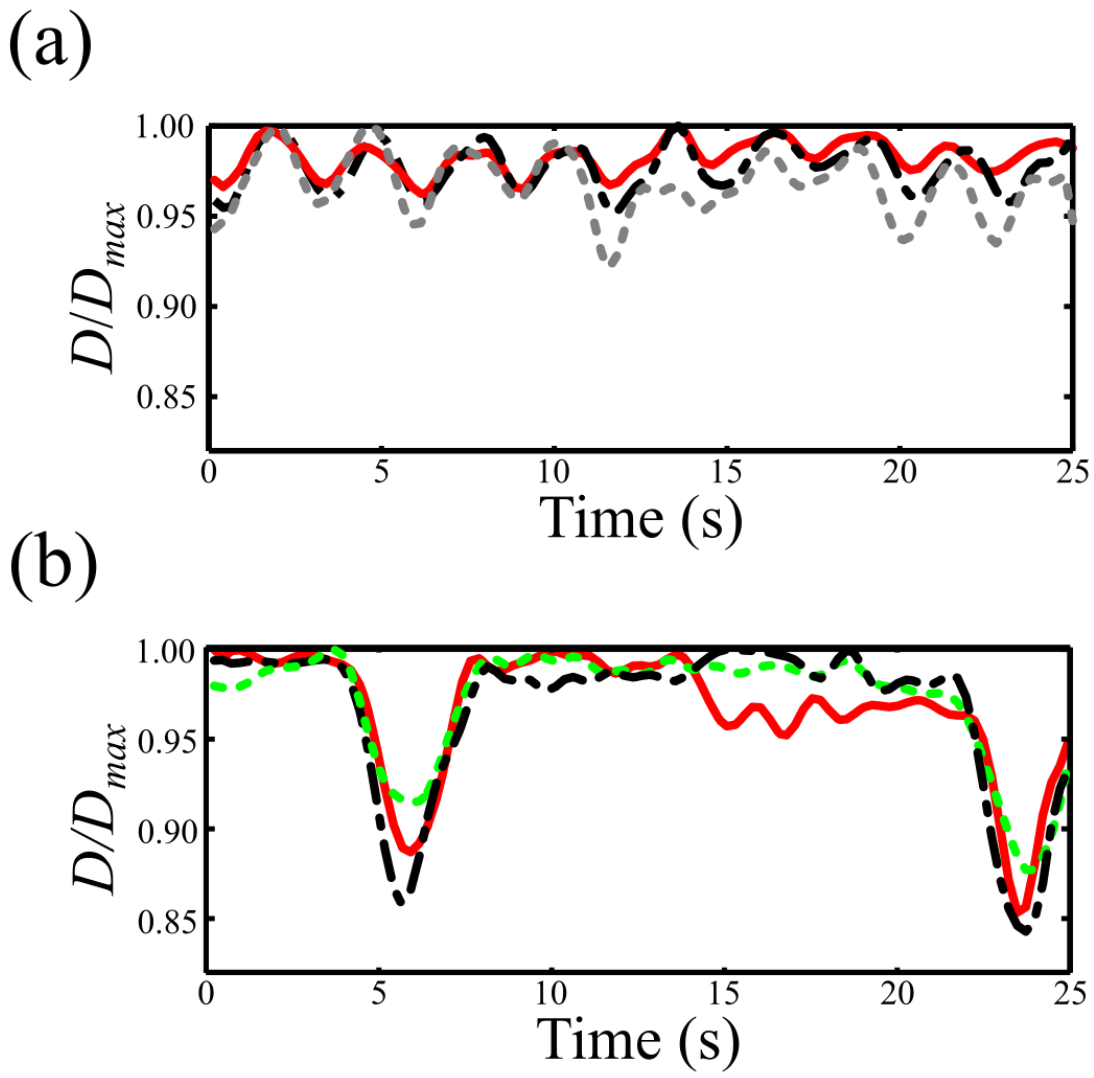

Figure 14: ***(a)*** **Changes in vessel diameter (D) in WT Mouse at three segments for 25 seconds. Red (solid) curve depicts the segment downstream of the normal bi-leaflet valve, gray (dashed) and black (double-dashed) curves represent the segments at center of the lymphangions;** ***(b)*** **Changes in vessel diameter (D) in MV Mouse at three segments for 25 seconds. Red (solid) curve depicts the segment downstream of the bi-leaflet valve, green (dashed) curve depicts the segment downstream of the uni-leaflet valve and black (double-dashed) curve represents the segment at center of the lymphangion**

4.3 Fluid Velocity

Particle velocity of each tracked particle was computed in MATLAB as discussed in previous chapter. Radial velocity profile was plotted based on the streamwise velocity *u* values of each particle within the segment. The particles within the segment were assumed to be positioned at the center plane of the segment, the plane at which diameter was calculated. Based on the particle velocities, velocity values were plotted and marked as solid dots in Figure 15. Higher order spline curve fits were used for curve representations of the velocity profile as shown in Figure 15.

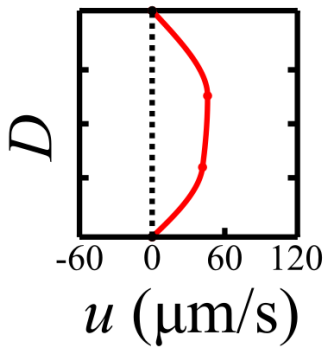

Figure 15: Sample velocity profile. The solid points on the curve represent the actual streamwise velocity value (*u*) of the particles in the segment. The red curve represents a spline curve fit.

The aggregate velocity *U* in the plane was computed by integration of fitted velocity curve profile. This technique was implemented to calculate U for all the defined segments at each of 750-time points spanning 25 seconds.

Linear flow rate of the fluid Q^* was defined as the product of velocity *u* to the diameter *D* of the segment.

$$Q^* = u^*D$$

The changes in the values of Q^* were compared for multiple segments and is shown in Figure 16. The values of Q^* are proportional to the values of U by the factor of vessel diameter. However due to challenges in particle tracking and presence of lesser number of particles at an instantaneous time points, U values could not be estimated. Q^* values represented in Figure 16 show the curve fit of Q^* values from the actual data. As seen in the figure, the velocity of the fluid is observed to have negative values as well. The negative values of U or Q^* implies retrograde flow within that segment. The flow in MV was observed to reverse even in the presence of valves – both normal and malformed. The flow was observed to be reversing in the valvular segment as well which showcases the presence of inter-lymphangion retrograde flow even in presence of valves. The differences in magnitudes of the flow rate varied for different cases and it is just an account of heterogeneity of the lymphatic system.

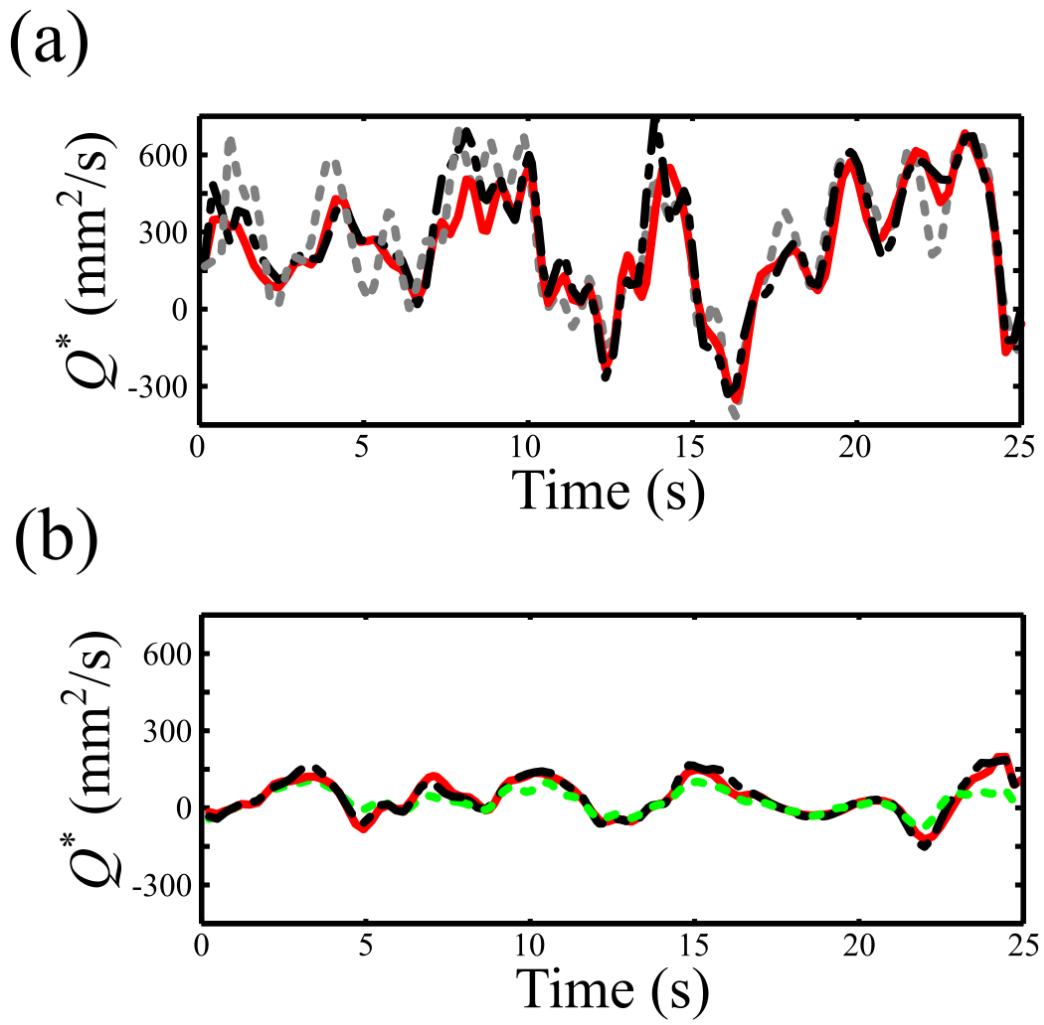

Figure 16: Changes in flow rate (Q^*) at three segments for 25 seconds in (a) WT Mouse - Red (solid) curve depicts the segment downstream of the normal bi-leaflet valve, gray (dashed) and black (double-dashed) curves represent the segment at center of the lymphangions; (b) MV Mouse - Red (solid) curve depicts the segment downstream of the bi-leaflet valve, green (dashed) curve depicts the segment downstream of the uni-leaflet valve and black (double-dashed) curve represents the segment at center of the lymphangion

4.4 Flow Cycles

Individual flow cycles were selected starting with first point that flow reverses until it reverses again. The temporal span of flow cycles T_{cycle} varies for each mouse and varies differently for each segment in a mouse vessel. This highlights the heterogeneity in lymphatic flow. The absence of a pumping organ is the primary contributing factor for this irregularity.

Different flow cycles were identified and T_{cycle} was found to be different in all the cycles. For comparison of cycles in different segments and different mouse cases, a new term (τ) was defined. τ rescales all the flow cycles from 0 to 1. Zero value of τ defines the start of flow cycle (retrograde flow) and one defines the end of flow cycle.

$$\tau = \frac{\mathbf{T - min(Tcycle)}}{\mathbf{max\ (Tcycle) - min(Tcycle)}}$$

One cycle was selected for both WT and MV Mice. The values of velocity *u* over the span of this cycle can be seen in Figure 17. The differences in time of each time cycle was overcome by changing the time scale from time in seconds to τ as defined previously. Segment 3 from WT Mouse was not considered in this analysis due to lesser number of particles in the segment and particles being out of focus. For both cases, the antegrade flow direction dominated implying a net forward flow in both cases.

To study the localized effects in each segment over the cycle, we calculated the velocity profiles (as discussed earlier) at five values of τ: 0.0, 0.25, 0.5, 0.75, 1.0 for each cycle. The diameter was normalized to compare the nature of the velocity profile. The

diameter of vessel changes over the cycle span for both mice as seen in previous section. The diameter was normalized as follows:

$$D^* = \frac{D - min(D)}{max\,(D) - min(D)}$$

where D^* ranges from 0 to 1. A value of 1 represents the largest diameter for that segment and corresponding to maximal vessel dilation. A value of zero for D^* implies the vessel walls are touching. The velocity profiles for five time points were plotted with respect to D^* for two cases and is shown in Figure 18.

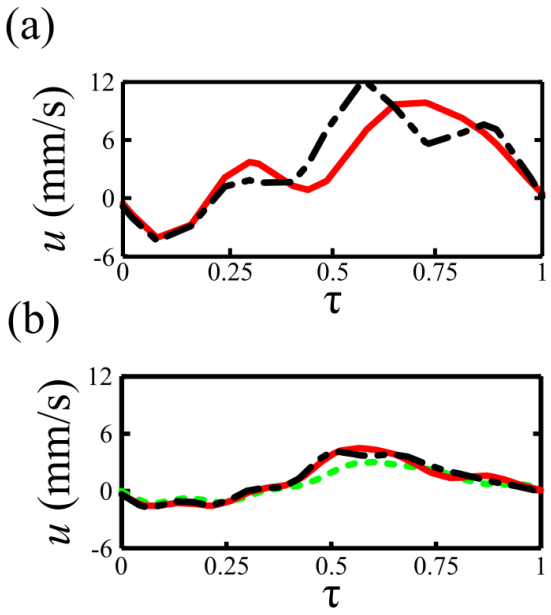

Figure 17: One flow cycle at segments. (a) WT Mouse - Red (solid) curve depicts the segment downstream of the normal bi-leaflet valve, black (double-dashed) curve represents the segment at center of the lymphangion, segment at the center of upstream lymphangion was ignored in this study due to absence of sufficient particles in the focal plane in that segment. (b) MV Mouse - Red (solid) curve depicts the segment downstream of the bi-leaflet valve, green (dashed) curve depicts the segment downstream of the uni-leaflet valve and black (double-dashed) curve represents the segment at center of the lymphangion

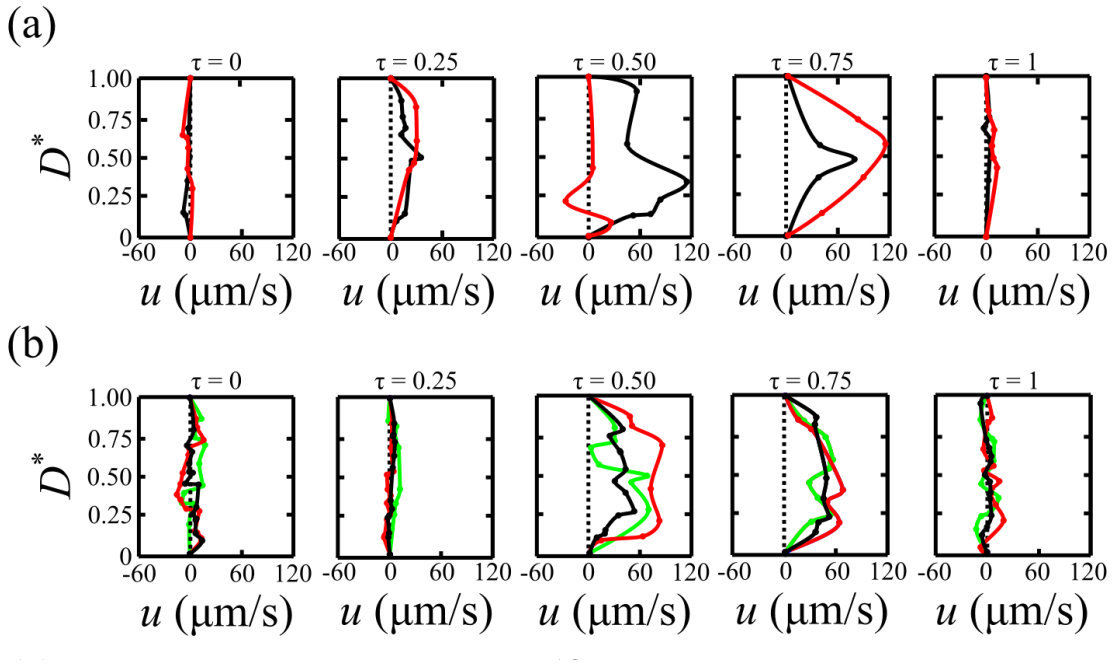

Figure 18: Velocity profiles at the segments at five time points (τ = 0.0, 0.25, 0.5, 0.75, 1.0) within one cycle. The solid points show the actual *u* value of the particles. The solid curve represents spline fit. (a) WT Mouse - Red curve depicts the segment downstream of the normal bi-leaflet valve, black curve represents the segment at center of the lymphangion; (b) MV Mouse - Red curve depicts the segment downstream of the bi-leaflet valve, green curve depicts the segment downstream of the uni-leaflet valve and black curve represents the segment at center of the lymphangion

At τ = 0, as seen in Figure 17, the flow is transitioning from forward flow to backward flow. The velocity values are closer to zero in all segments. The velocity profile is more parabolic at τ = 0.5. The profile becomes further parabolic at the valvular segment (Red curve) in WT Mouse at τ = 0.75. The region downstream of the normal valve (Red curve) in MV Mouse shows a more parabolic profile in comparison to region downstream of malformed valve (Green curve).

4.5 Flow Cycle Universality

Figure 19 shows two flow cycles each for the three segments in WT Mouse. Thus, the total number of flow cycles plotted are six. Curve peaks were found to properly shift the curves such that (t/t_{cycle}) = 0 corresponds to the maximum peak of each curve. The maximum u value of multiple peaks (U_{max}) differed in amplitude. Interestingly, the lowest cycle-U_{max} was 50% of the highest value of $U_{max.}$ Thus, adding another key finding to the observation of heterogeneity of lymphatic flow cycles. Figure 19a shows u/U_{max} plotted on t/t_{cycle} scale and peaks shifted to zero for WT.

Similarly, three flow cycles each for three segments in MV were plotted using the same methods described before (Figure 19b). Thus, 9 flow cycles were considered for MV Mouse for this study.

The u values for all the cycles for each mouse were averaged such that one curve was generated representing the average of all the flow cycles. Analysis was performed on these two averaged curves based on methodology shown in Figure 20. The time scale t was rescaled to t/t_0, where t_0 is difference in time from peak (of u value: U_{max}) to time when the amplitude u_0 is 50% of the amplitude u_0 as shown in Figure 20. Velocity u was normalized on scale of from 0 to 1 as follows:

$$\boldsymbol{u^*} = \frac{\mathbf{u - min(u)}}{\mathbf{max\,(u) - min(u)}} = \frac{\mathbf{u - min(u)}}{\boldsymbol{u0}}$$

A value of zero on the normalized velocity scale can also imply retrograde flow.

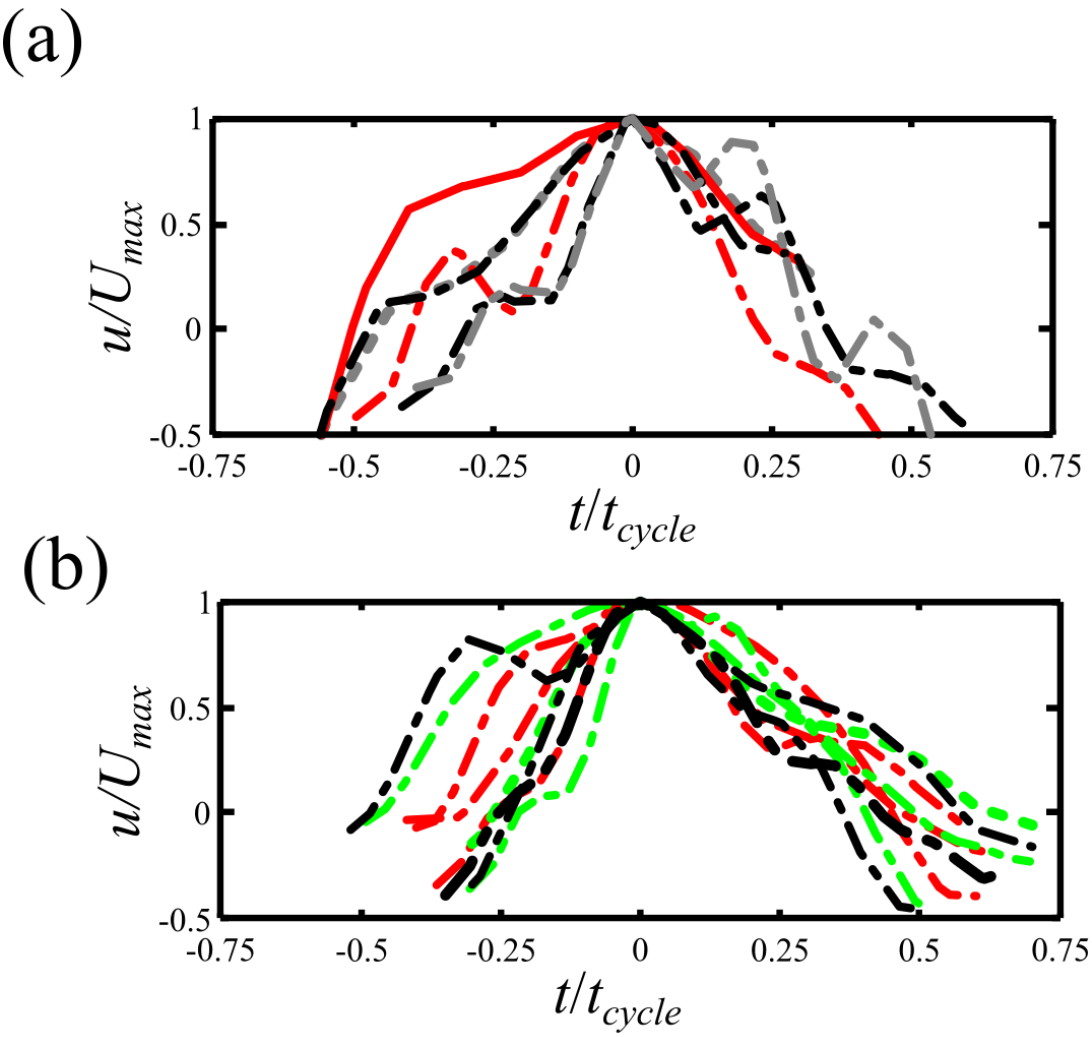

Figure 19: Multiple flow cycles (u/U_{max}) within one animal at different segments plotted on a normalized time scale (t/t_{cycle}), curve peaks shifted such that (t/t_{cycle}) = 0. (a) Six flow cycles from three segments in WT Mouse; (b) Nine flow cycles from three segments in MV Mouse

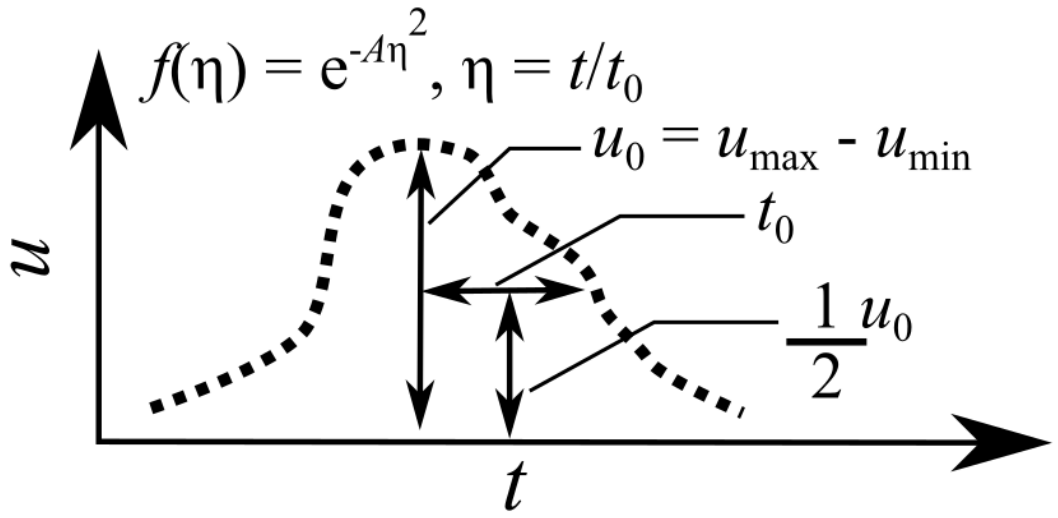

Figure 20: Universality function analysis methodology. The dotted line represents a sample average flow cycle depicting multiple flow cycles within the same animal.

The two averaged cycles were then plotted using a t/t_0 time scale. A Gaussian curve fitting method was used to find the best curve representing the average of these two curves by optimizing the errors as shown in the black curve in Figure 21. The function $f(\eta) = e^{-0.95\,\eta 2}$ represents a potential universal lymphatic flow curve.

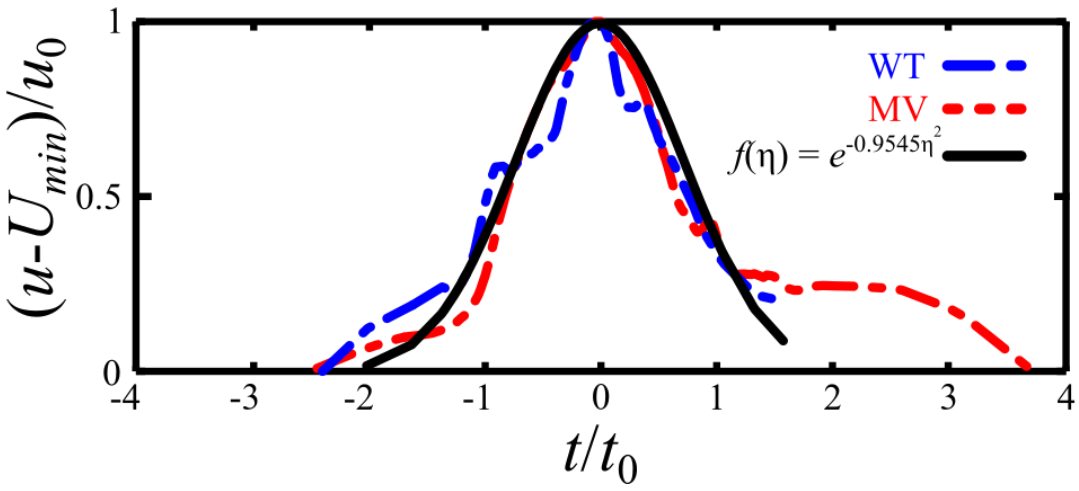

Figure 21: Lymphatic universal flow cycle function. The blue curve represents the average flow cycle for WT Mouse. The red curve represents the average flow cycle for MV Mouse. The solid black curve shows a Gaussian curve fit for the two curves.

4.6 Particle Trajectory

A particle located in a valve recirculation zone, a particle travelling in the vessel lumen and particle in contact with the valve surface were considered for a trajectory study comparison in WT and MV. The length of time corresponding to the tracking of these particles was one flow cycle, the same flow cycle previously selected. Wall shear stress values were calculated whenever the particle was in contact with the wall. Figure 22 shows the trajectory of the particles and the estimated WSS. The hollow circles in the trajectory plots represents the particle moving in the antegrade direction and the solid dots represent retrograde travel.

The particle moving in the vessel lumen and traveling over the normal valve surface in WT Mouse during intra-lymphangion transport traveled the most and covered roughly 100 microns. On the other hand, displacement of similar particle in MV Mouse

traveling over the uni-leaflet valve was roughly 15 microns. Interestingly, a particle moving and in contact with the endothelium on the vessel wall (Blue) travelled a longer distance than the particle in the lumen (Black) in the case of MV (Figure 22d). The WSS was higher on both valve and vessel wall endothelium in WT Mouse in comparison to MV Mouse potentially affecting differential gene expression in the endothelium.

The valve, both uni-leaflet and bi-leaflet, promote a fluid recirculation zone beneath the leaflets. It was observed that particles in this region do not displace and recirculate in form of eddies in that region. The trajectory of two such particles – one underneath each valve was studied. It could be seen in all trajectory plots that the particle followed the same path during flow reversal as during forward flow (Figure 22). This is characteristic of low Reynolds number flow and lymph flow has very low Reynolds number as detailed in Chapter 1.

The presence of a single leaflet valve affected the overall inter-lymphangion transport of the fluid in comparison to a normal bi-leaflet valve. Localized slower transport of lymph can affect the fluid accumulation in the upstream. If this type of valvular is more widespread, it could potentially lead to retarded lymph transport - lymphedema.

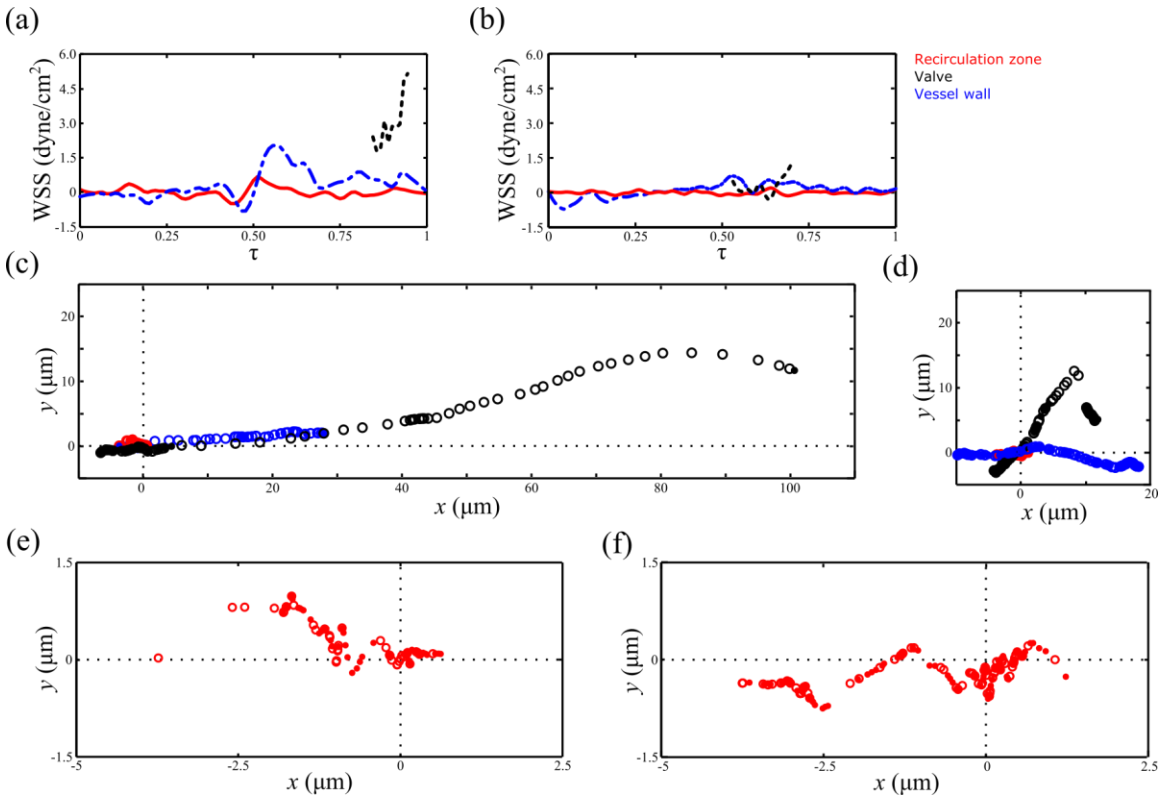

Figure 22: Comparison of trajectories of three particles within the vessel for span of one flow cycle. The selected particles were in recirculation zone (Red), along the vessel wall (Blue) and traveling over the valve surface (Black). Wall shear stress (WSS) experienced by three particles of different trajectories in WT Mouse (a) and MV Mouse (b); Trajectory of three particles in WT Mouse (c) and MV Mouse (d). Hollow circles represent antegrade direction whereas solid circles represent retrograde direction of travel; (e) Trajectory of a particle within the recirculating zone of normal bi-leaflet valve in WT Mouse; (f)Trajectory of a particle within the recirculating zone of malformed uni-leaflet valve in MV Mouse

4.7 Comparison of Flow Fields in a Flow Cycle

Interpolated data of the velocities was compared at five points in the cycles with no slip condition at the vessel and valve edges. The time points were same as used in previous studies; τ = 0.0, 0.25, 0.5, 0.75 and 1.0. Figures 23 and 24 show the velocity vector fields in the lymphatic vessels for WT Mouse and MV Mouse respectively.

It can be observed that the flow reversal is faster in the valves than in the lymphangions. Higher velocities are observed at the center of the vessel lumen. WT Mouse has higher fluid velocity in comparison to MV Mouse, showing heterogeneity of lymphatics in different animals.

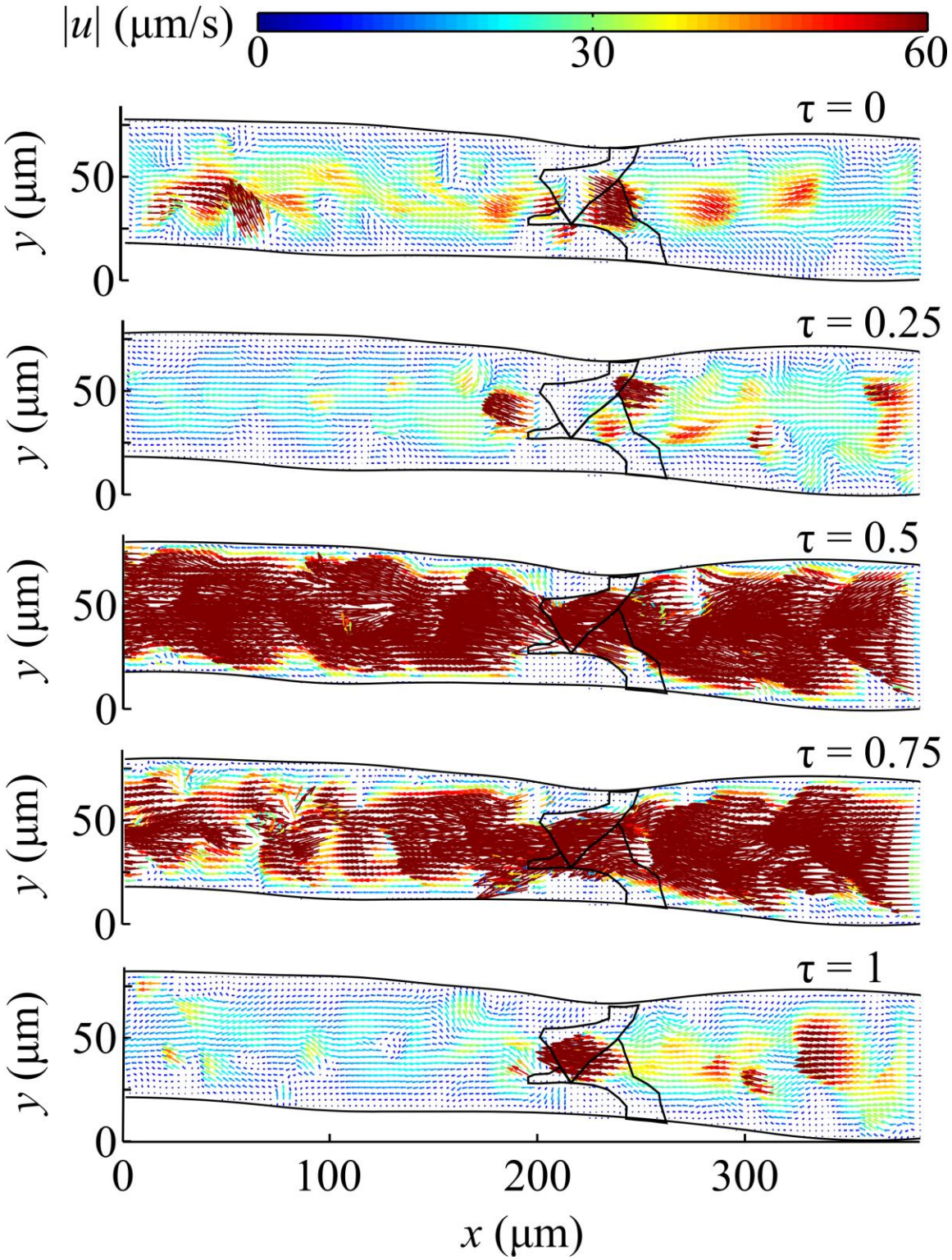

Figure 23: Vector plots depicting the flow field at various times in the flow cycle (τ = 0.0, 0.25, 0.5, 0.75, 1.0) for WT Mouse.

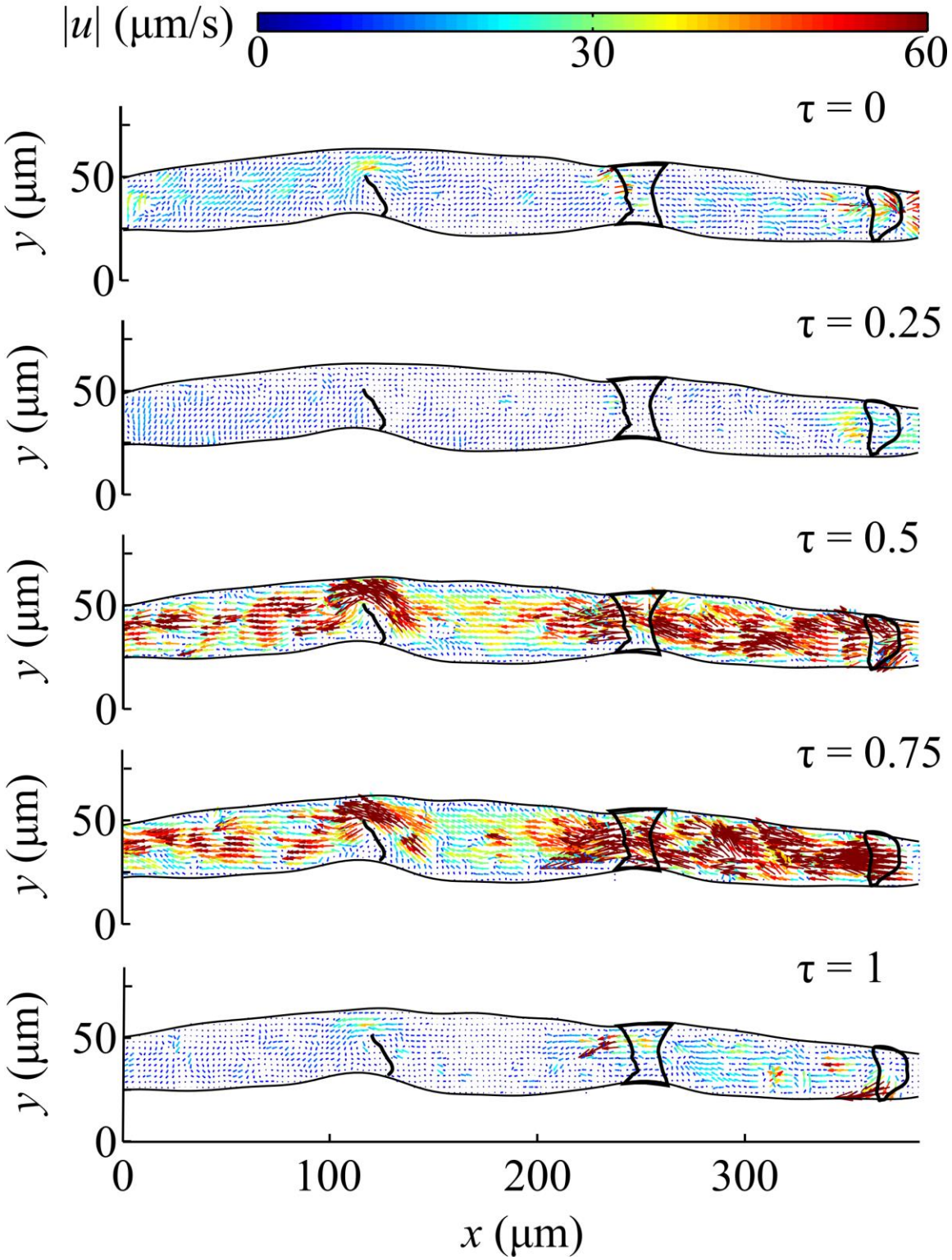

Figure 24: Vector plots depicting the flow field at various times in the flow cycle (τ = 0.0, 0.25, 0.5, 0.75, 1.0) for MV Mouse

In Figure 24, for MV Mouse, at τ = 0.5 and 0.75, when the fluid is transported forward towards the venous system, higher fluid flow is observed from the lymphangion upstream of a normal valve than from the lymphangion upstream of the unileaflet valve. This suggests the possiblity of fluid obstruction due to single leaflet valve. Also, it can be observed that at τ = 0.5 and 0.75, higher velocities are experienced closer to the vessel wall due to the malformed valve. Thus, affecting the stresses experienced by LECs in that region.

WSS was computed at the segments defined previously in both WT Mouse and MV Mouse. Figure 25 shows the values of WSS in these segments at both top surface and bottom surfaces of the vessels. The WSS magnitude values was within 1.2 dyne/cm^2. It can be noted that the higher values of WSS was observed when the flow rate was higher (τ = 0.5, 0.75).

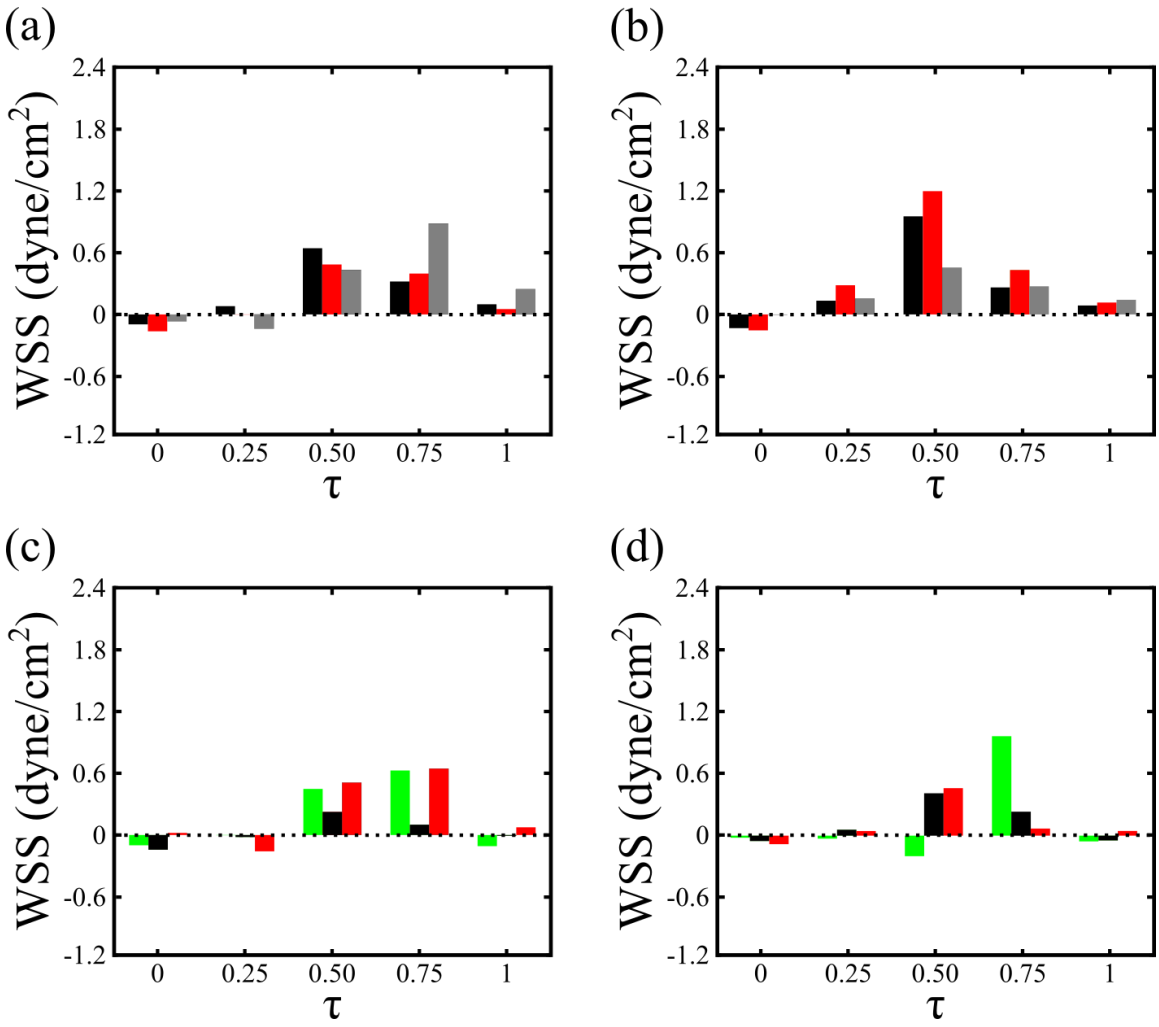

Figure 25: Vessel Wall Shear Stress (WSS) from interpolated velocity data at five time points (τ = 0.0, 0.25, 0.5, 0.75, 1.0) in the flow cycle. (a, b) WSS calculated at top and bottom edge of the vessel respectively in three segments for WT Mouse. Red bar depicts the segment downstream of the normal bi-leaflet valve, gray and black bars represent the segments at center of the lymphangions; (c, d) WSS calculated at top and bottom edge of the vessel respectively in three segments for MV Mouse - Red bar depicts the segment downstream of the bi-leaflet valve, green bar depicts the segment downstream of the uni-leaflet valve and black bar represents the segment at center of the lymphangion

4.8 Vorticity and Strain Fields

Vorticity describes the spinning motion experienced by the lymph. Figure 26 and 27 shows the vorticity field in the vessels for WT Mouse and MV Mouse at five time-points in the flow cycle. The positive and negative signs describe the direction of spinning. Higher vorticity regions were observed near the valves in both WT and MV Mice. Higher flow rate (τ = 0.5, 0.75) promote higher vorticity regions in the vessels. Higher vorticity regions can potentially be regions for flow separation and are mostly seen downstream of the valves.

The fluid deformation represented by normal and shear strain is represented in Figures 28, 29, 30 and 31 for both cases. Narrowing of vessel within the valve regions promote higher normal and shear strain fields as seen in the figures.

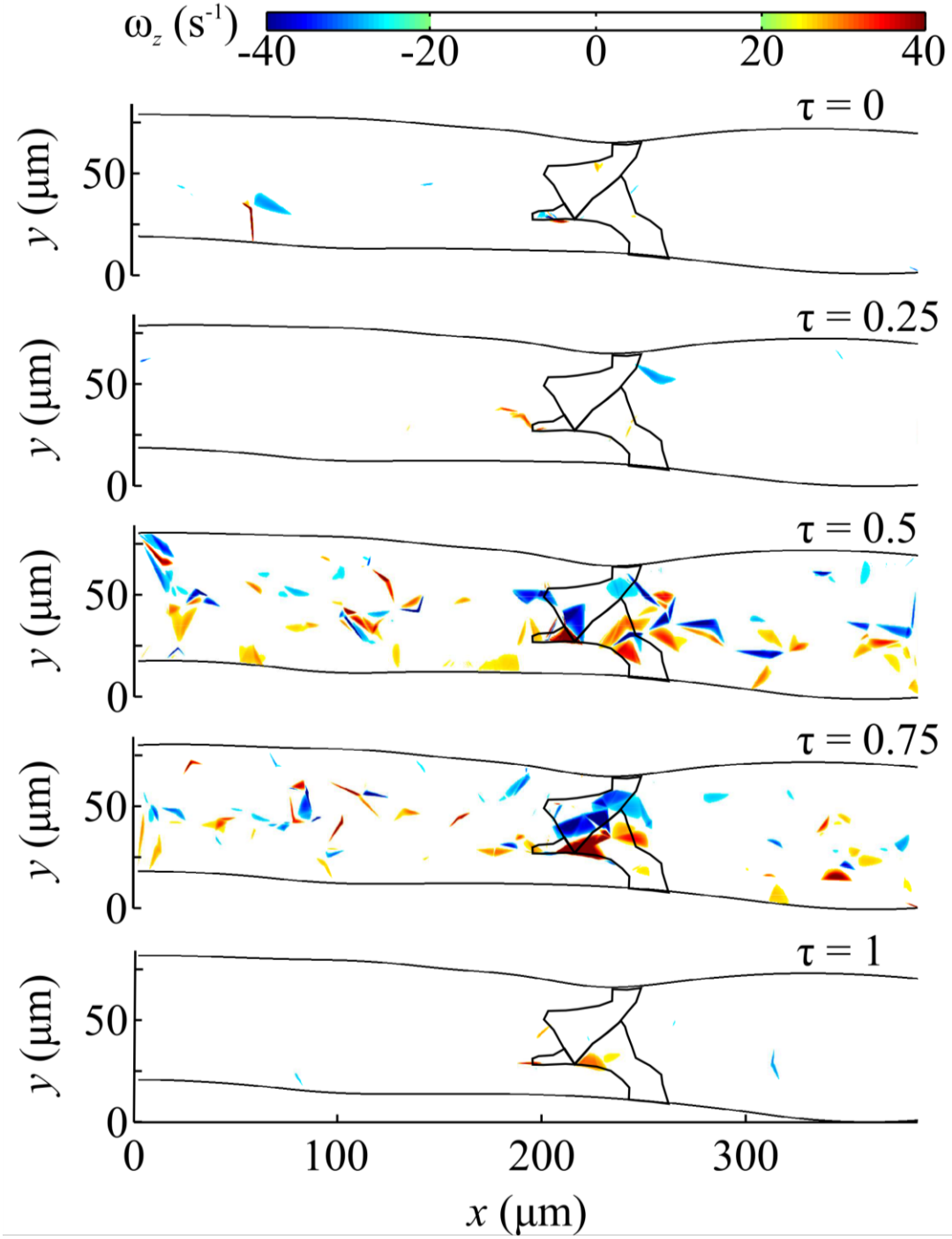

Figure 26: Vorticity field within the vessel at various times in a flow cycle (τ = 0.0. 0.25. 0.5, 0.75, 1.0) for WT Mouse

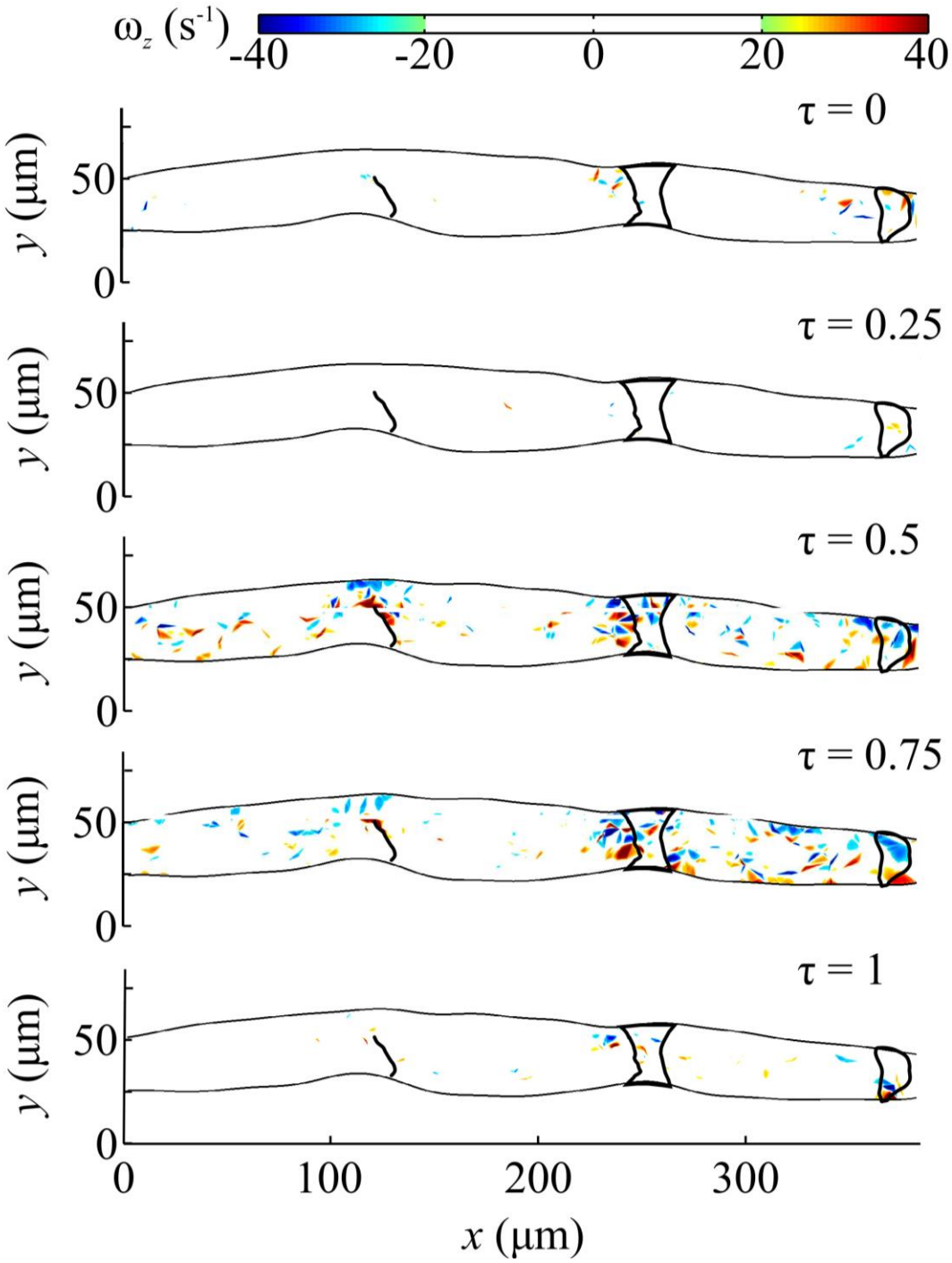

Figure 27: Vorticity field within the vessel at various times in a flow cycle (τ = 0.0. 0.25. 0.5, 0.75, 1.0) for MV Mouse

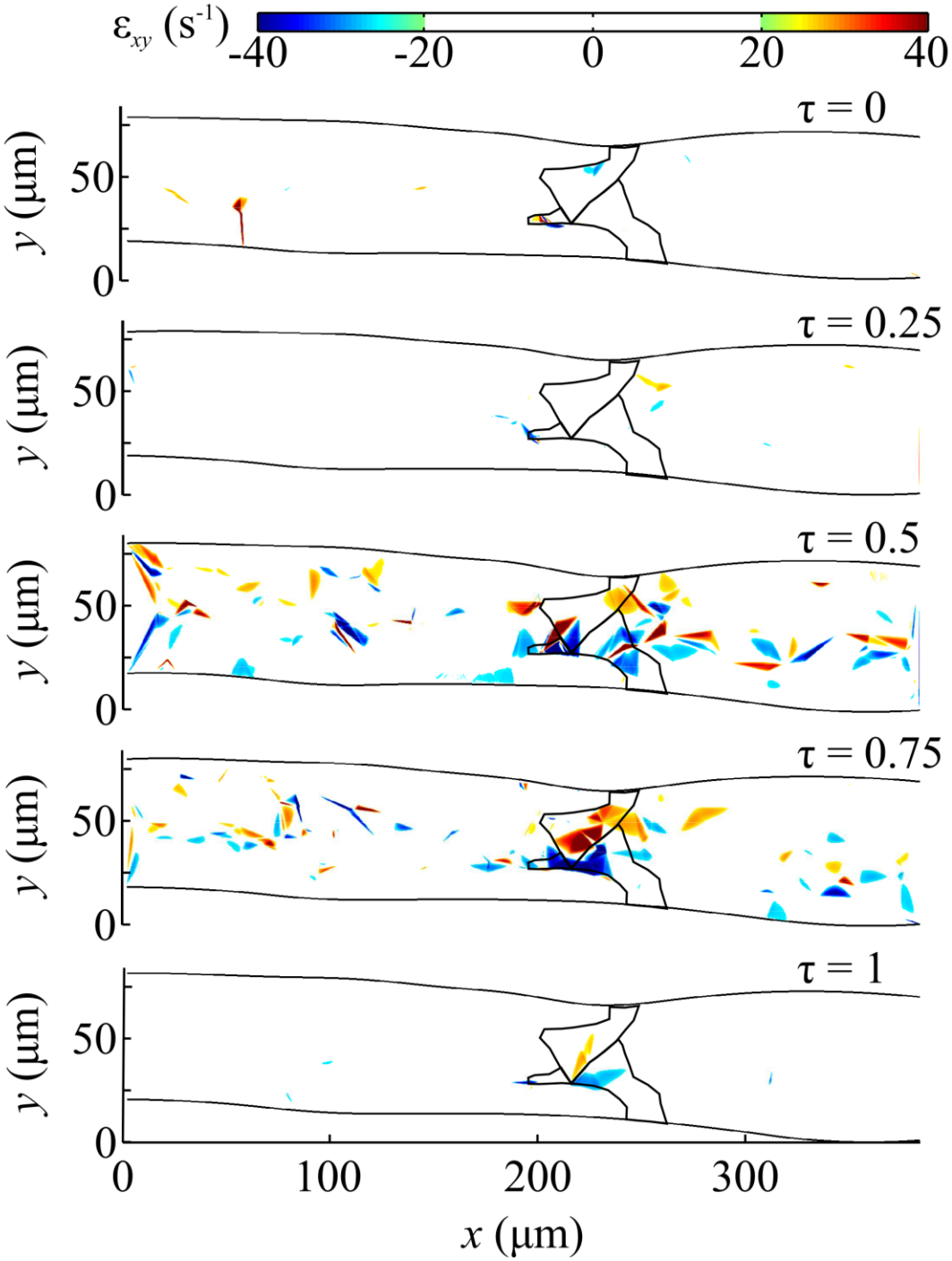

Figure 28: Normal strain field within the vessel at various times in a flow cycle (τ = 0.0. 0.25. 0.5, 0.75, 1.0) for WT Mouse

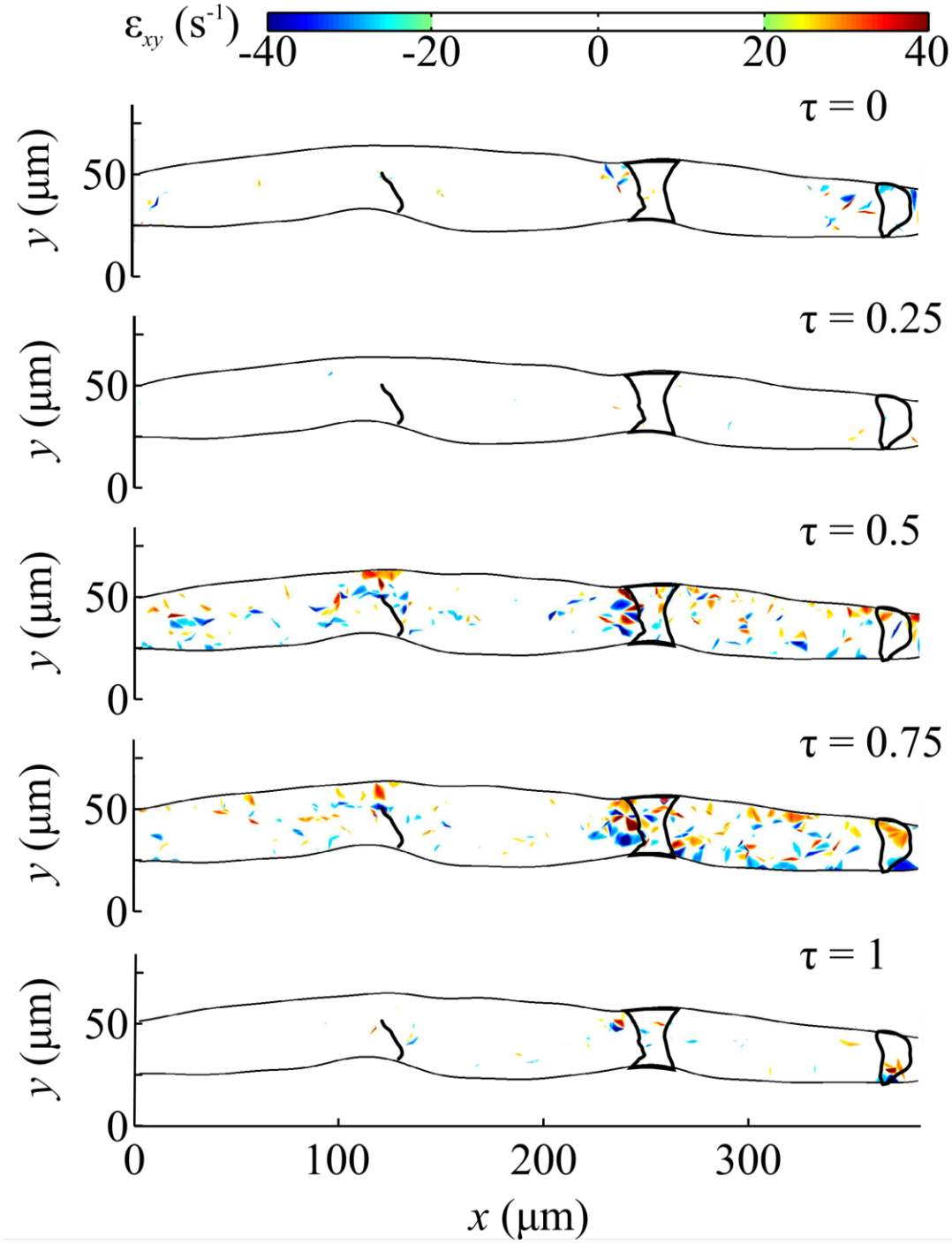

Figure 29: Normal strain field within the vessel at various times in a flow cycle (τ = 0.0. 0.25. 0.5, 0.75, 1.0) for MV Mouse

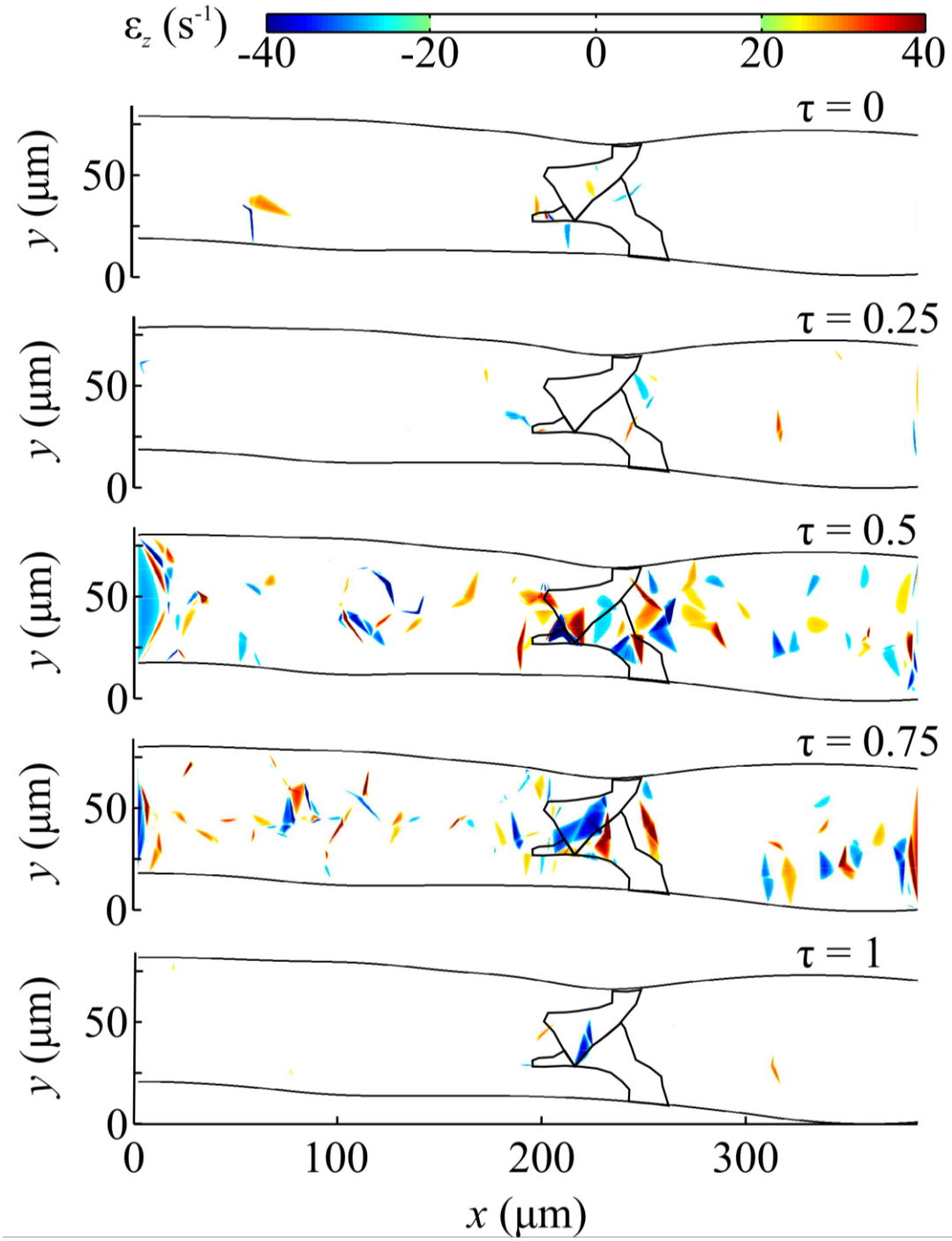

Figure 30: Shear strain field within the vessel at various times in a flow cycle (τ = 0.0. 0.25. 0.5, 0.75, 1.0) for WT Mouse

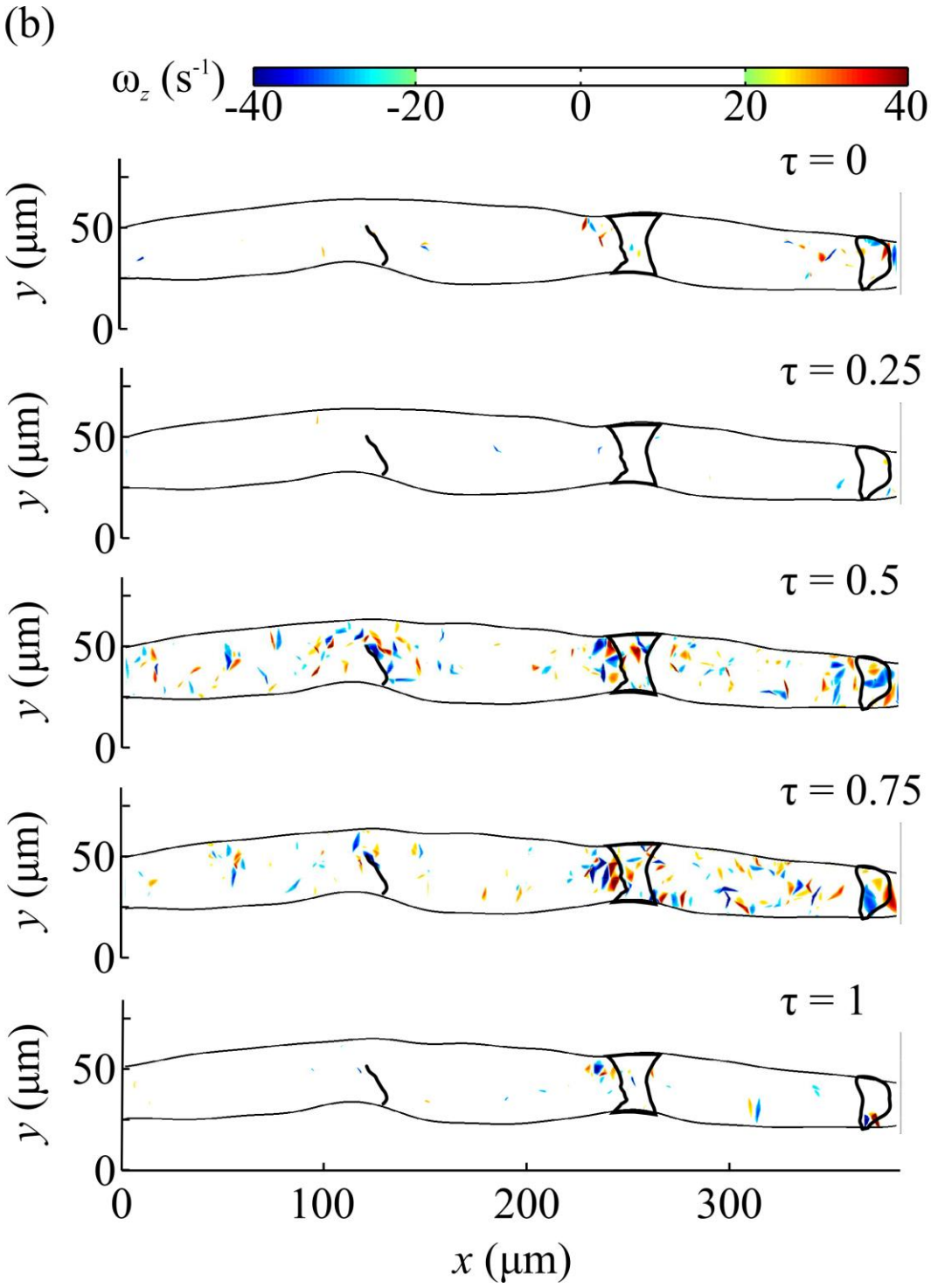

Figure 31: Shear strain field within the vessel at various times in a flow cycle (τ = 0.0. 0.25. 0.5, 0.75, 1.0) for MV Mouse

CHAPTER 5

CONCLUSION

This study explores the effects of a single leaflet valve in wild-type mouse lymphatic vessels by studying the lymph transport *in vivo*. Presence of retrograde was observed flow in wild-type mice models even in presence of valves. The lymphatic system is a complex network of smaller initial and pre-collecting lymphatics and larger collecting lymphatics. Thus, it should be noted that flow of particles was studied in just one of these vessels among a complex network of lymphatic vessels.

Initial immunohistochemistry experiments failed to show signals for both PROX-1 and eNOS. Increasing the permeabilization time helped with PROX-1 signal. This way, the lymphatic network could be identified. However, localized expression of eNOS on LECs was not clearly observed. This experiment can be performed to study the presence of different protein expressions within the same vessel.

Future works include studying the flow and effects of flow in genetically modified models. Lymphocytes can be labeled instead of injecting particles, to further enhance our understanding of lymph transport *in vivo*. Also, increasing the sampling size can help understand the effects of malformation in better way. The universality flow function computed in this study can also be verified for by increasing the sampling size, both looking at different mouse models and different regions within the same animal.

BIBLIOGRAPHY

[1] M. A. Swartz, "The physiology of the lymphatic system," *Adv. Drug Deliv. Rev.*, vol. 50, no. 1, pp. 3–20, Aug. 2001.

[2] M. Földi and R. H. K. Strössenreuther, *Foundations of Manual Lymph Drainage*. Elsevier Health Sciences, 2004.

[3] T. Tammela and K. Alitalo, "Lymphangiogenesis: Molecular Mechanisms and Future Promise," *Cell*, vol. 140, no. 4, pp. 460–476, Feb. 2010.

[4] M. A. Swartz and M. Skobe, "Lymphatic function, lymphangiogenesis, and cancer metastasis," *Microsc. Res. Tech.*, vol. 55, no. 2, pp. 92–99, Oct. 2001.

[5] L. V. Leak and J. F. Burke, "Ultrastructural Studies on the Lymphatic Anchoring Filaments," *J. Cell Biol.*, vol. 36, no. 1, pp. 129–149, Jan. 1968.

[6] C. Danussi *et al.*, "Emilin1 Deficiency Causes Structural and Functional Defects of Lymphatic Vasculature," *Mol. Cell. Biol.*, vol. 28, no. 12, pp. 4026–4039, Jun. 2008.

[7] H. Maby-El Hajjami and T. V. Petrova, "Developmental and pathological lymphangiogenesis: from models to human disease," *Histochem. Cell Biol.*, vol. 130, no. 6, pp. 1063–1078, Dec. 2008.

[8] M. C. Mazzoni, T. C. Skalak, and G. W. Schmid-Schönbein, "Structure of Lymphatic Valves in the Spinotrapezius Muscle of the Rat," *J. Vasc. Res.*, vol. 24, no. 6, pp. 304–312, 1987.

[9] J. B. Dixon, S. T. Greiner, A. A. Gashev, G. L. Cote, J. E. Moore, and D. C. Zawieja, "Lymph Flow, Shear Stress, and Lymphocyte Velocity in Rat Mesenteric Prenodal Lymphatics," *Microcirculation*, vol. 13, no. 7, pp. 597–610, Jan. 2006.

[10] G. Sacchi, E. Weber, M. Agliano, N. Raffaelli, and L. Comparini, "The structure of superficial lymphatics in the human thigh: precollectors," *Anat. Rec.*, vol. 247, no. 1, pp. 53–62, Jan. 1997.

[11] M. Jeltsch, T. Tammela, K. Alitalo, and J. Wilting, "Genesis and pathogenesis of lymphatic vessels," *Cell Tissue Res.*, vol. 314, no. 1, pp. 69–84, Oct. 2003.

[12] R. P. Boggon and A. J. Palfrey, "The microscopic anatomy of human lymphatic trunks.," *J. Anat.*, vol. 114, no. Pt 3, pp. 389–405, Apr. 1973.

[13] K. P. Arkill, J. Moger, and C. P. Winlove, "The structure and mechanical properties of collecting lymphatic vessels: an investigation using multimodal nonlinear microscopy," *J. Anat.*, vol. 216, no. 5, pp. 547–555, May 2010.

[14] F. Abtahian *et al.*, “Regulation of Blood and Lymphatic Vascular Separation by Signaling Proteins SLP-76 and Syk,” *Science*, vol. 299, no. 5604, pp. 247–251, Jan. 2003.

[15] E. Kriehuber *et al.*, “Isolation and Characterization of Dermal Lymphatic and Blood Endothelial Cells Reveal Stable and Functionally Specialized Cell Lineages,” *J. Exp. Med.*, vol. 194, no. 6, pp. 797–808, Sep. 2001.

[16] P. Saharinen, T. Tammela, M. J. Karkkainen, and K. Alitalo, “Lymphatic vasculature: development, molecular regulation and role in tumor metastasis and inflammation,” *Trends Immunol.*, vol. 25, no. 7, pp. 387–395, Jul. 2004.

[17] N. Wick *et al.*, “Lymphatic Precollectors Contain a Novel, Specialized Subpopulation of Podoplaninlow, CCL27-Expressing Lymphatic Endothelial Cells,” *Am. J. Pathol.*, vol. 173, no. 4, pp. 1202–1209, Oct. 2008.

[18] J. Keuschnigg *et al.*, “Plasticity of Blood- and Lymphatic Endothelial Cells and Marker Identification,” *PLoS ONE*, vol. 8, no. 9, p. e74293, Sep. 2013.

[19] G. Jurisic and M. Detmar, “Lymphatic endothelium in health and disease,” *Cell Tissue Res.*, vol. 335, no. 1, pp. 97–108, Jan. 2009.

[20] G. Oliver and M. Detmar, “The rediscovery of the lymphatic system: old and new insights into the development and biological function of the lymphatic vasculature,” *Genes Dev.*, vol. 16, no. 7, pp. 773–783, Apr. 2002.

[21] T. V. Petrova *et al.*, “Lymphatic endothelial reprogramming of vascular endothelial cells by the Prox-1 homeobox transcription factor,” *EMBO J.*, vol. 21, no. 17, pp. 4593–4599, Sep. 2002.

[22] T. Mäkinen *et al.*, “PDZ interaction site in ephrinB2 is required for the remodeling of lymphatic vasculature,” *Genes Dev.*, vol. 19, no. 3, pp. 397–410, Feb. 2005.

[23] D. T. Sweet *et al.*, “Lymph flow regulates collecting lymphatic vessel maturation in vivo,” *J. Clin. Invest.*, vol. 125, no. 8, pp. 2995–3007, Aug. 2015.

[24] P.-Y. Von Der Weid, “Review article: lymphatic vessel pumping and inflammation—the role of spontaneous constrictions and underlying electrical pacemaker potentials,” *Aliment. Pharmacol. Ther.*, vol. 15, no. 8, pp. 1115–1129, Aug. 2001.

[25] S. Liao *et al.*, “Impaired lymphatic contraction associated with immunosuppression,” *Proc. Natl. Acad. Sci.*, vol. 108, no. 46, pp. 18784–18789, Nov. 2011.

[26] L. A. Barouch *et al.*, “Nitric oxide regulates the heart by spatial confinement of nitric oxide synthase isoforms,” *Nature*, vol. 416, no. 6878, pp. 337–339, Mar. 2002.

[27] C. Kunert, J. W. Baish, S. Liao, T. P. Padera, and L. L. Munn, “Mechanobiological oscillators control lymph flow,” *Proc. Natl. Acad. Sci. U. S. A.*, vol. 112, no. 35, pp. 10938–10943, Sep. 2015.

[28] Y. C. Boo *et al.*, “Shear Stress Stimulates Phosphorylation of Endothelial Nitric-oxide Synthase at Ser1179 by Akt-independent Mechanisms ROLE OF PROTEIN KINASE A,” *J. Biol. Chem.*, vol. 277, no. 5, pp. 3388–3396, Feb. 2002.

[29] M. J. Davis, E. Rahbar, A. A. Gashev, D. C. Zawieja, and J. E. Moore, “Determinants of valve gating in collecting lymphatic vessels from rat mesentery,” *Am. J. Physiol. - Heart Circ. Physiol.*, vol. 301, no. 1, pp. H48–H60, Jul. 2011.

[30] E. Bazigou and T. Makinen, “Flow control in our vessels: vascular valves make sure there is no way back,” *Cell. Mol. Life Sci.*, vol. 70, no. 6, pp. 1055–1066, Mar. 2013.

[31] S. H. Lee, H. J. Wen, and C. L. Shen, “Ultrastructure of the monkey thoracic duct and the cisterna chyli.,” *J. Anat.*, vol. 182, no. Pt 2, pp. 205–212, Apr. 1993.

[32] S. G. Rockson, “Lymphedema,” *Curr. Treat. Options Cardiovasc. Med.*, vol. 8, no. 2, pp. 129–136, Mar. 2006.

[33] M. H. Witte, M. J. Bernas, C. P. Martin, and C. L. Witte, “Lymphangiogenesis and lymphangiodysplasia: From molecular to clinical lymphology,” *Microsc. Res. Tech.*, vol. 55, no. 2, pp. 122–145, Oct. 2001.

[34] J. B. Dixon, “Lymphatic lipid transport: sewer or subway?,” *Trends Endocrinol. Metab.*, vol. 21, no. 8, pp. 480–487, Aug. 2010.

[35] R. H. Mellor *et al.*, “Mutations in FOXC2 Are Strongly Associated With Primary Valve Failure in Veins of the Lower Limb,” *Circulation*, vol. 115, no. 14, pp. 1912–1920, Apr. 2007.

[36] E. Bazigou *et al.*, “Integrin-α9 Is Required for Fibronectin Matrix Assembly during Lymphatic Valve Morphogenesis,” *Dev. Cell*, vol. 17, no. 2, pp. 175–186, Aug. 2009.

[37] A. Irrthum *et al.*, “Mutations in the Transcription Factor Gene SOX18 Underlie Recessive and Dominant Forms of Hypotrichosis-Lymphedema-Telangiectasia,” *Am. J. Hum. Genet.*, vol. 72, no. 6, pp. 1470–1478, Jun. 2003.

[38] M. R. Saban *et al.*, “Visualization of lymphatic vessels through NF-κB activity,” *Blood*, vol. 104, no. 10, pp. 3228–3230, Nov. 2004.

[39] P. R. Hess *et al.*, “Platelets mediate lymphovenous hemostasis to maintain blood-lymphatic separation throughout life,” *J. Clin. Invest.*, vol. 124, no. 1, pp. 273–284, Jan. 2014.

[40] K. Radhakrishnan and S. G. Rockson, “The Clinical Spectrum of Lymphatic Disease,” *Ann. N. Y. Acad. Sci.*, vol. 1131, no. 1, pp. 155–184, May 2008.

[41] W. D. Melrose, “Lymphatic filariasis: new insights into an old disease,” *Int. J. Parasitol.*, vol. 32, no. 8, pp. 947–960, Jul. 2002.

[42] K. M. Pfarr, A. Y. Debrah, S. Specht, and A. Hoerauf, “Filariasis and lymphoedema,” *Parasite Immunol.*, vol. 31, no. 11, pp. 664–672, Nov. 2009.

[43] C. Becker, J. Assouad, M. Riquet, and G. Hidden, “Postmastectomy Lymphedema,” *Ann. Surg.*, vol. 243, no. 3, pp. 313–315, Mar. 2006.

[44] G. W. Schmid-Schonbein, “Microlymphatics and lymph flow,” *Physiol. Rev.*, vol. 70, no. 4, pp. 987–1028, Oct. 1990.

[45] N. P. Reddy, T. A. Krouskop, and J. Paul H. Newell, “Biomechanics of a Lymphatic Vessel,” *J. Vasc. Res.*, vol. 12, no. 5, pp. 261–278, 1975.

[46] E. Rahbar and J. E. Moore, “A model of a radially expanding and contracting lymphangion,” *J. Biomech.*, vol. 44, no. 6, pp. 1001–1007, Apr. 2011.

[47] C. G. Caro, *The Mechanics of the Circulation*. Cambridge University Press, 2012.

[48] S. G. Rockson, “Current concepts and future directions in the diagnosis and management of lymphatic vascular disease,” *Vasc. Med.*, vol. 15, no. 3, pp. 223–231, Jun. 2010.

[49] K. N. Margaris and R. A. Black, “Modelling the lymphatic system: challenges and opportunities,” *J. R. Soc. Interface*, vol. 9, no. 69, pp. 601–612, Apr. 2012.

[50] Y. Xie, T. R. Bagby, M. Cohen, and M. L. Forrest, “Drug delivery to the lymphatic system: importance in future cancer diagnosis and therapies,” *Expert Opin. Drug Deliv.*, vol. 6, no. 8, pp. 785–792, Aug. 2009.

[51] E. Bourennane, P. Gouton, M. Paindavoine, and F. Truchetet, “Generalization of Canny–Deriche filter for detection of noisy exponential edge,” *Signal Process.*, vol. 82, no. 10, pp. 1317–1328, Oct. 2002.

[52] D. Watson, *Contouring: A Guide to the Analysis and Display of Spatial Data*. Elsevier, 2013.